Interplay of microbial communities with mineral environments in coralline algae

Patricia M. Valdespino-Castillo [a,1], Andrea Bautista-García [b,1], Fabio Favoretto [b,c], Martín Merino-Ibarra [d], Rocío J. Alcántara-Hernández [e], Teresa Pi-Puig [e,f], F. Sergio Castillo [d], Silvia Espinosa-Matías [g], Hoi-Ying Holman [a], Anidia Blanco-Jarvio [b,*]

[a] Molecular Biophysics and Integrated Bioimaging Division, Lawrence Berkeley National Laboratory, Berkeley, CA, United States
[b] Laboratorio de Bioingeniería y Ciencias Ambientales (BICA), Departamento Académico de Ingeniería en Pesquerías, Universidad Autónoma de Baja California Sur, La Paz, BCS, Mexico
[c] Gulf of California Marine Program, Scripps Institution of Oceanography, University of California San Diego, CA, United States
[d] Unidad Académica de Biodiversidad Acuática, Instituto de Ciencias del Mar y Limnología, Universidad Nacional Autónoma de México, Mexico City, Mexico
[e] Instituto de Geología, Universidad Nacional Autónoma de México, Mexico City, Mexico
[f] Laboratorio Nacional de Geoquímica y Mineralogía (LANGEM), Universidad Nacional Autónoma de México, Mexico City, Mexico
[g] Laboratorio de Microscopía Electrónica de Barrido, Facultad de Ciencias, Universidad Nacional Autónoma de México, Mexico City, Mexico

HIGHLIGHTS

- The interplay of microorganisms and algal mineral bioconstructions remains poorly understood.
- Carbonates rich in Fe and Mg found make CA relevant targets to study coastal resilience.
- Halophiles and evaporite minerals concurrently suggest halophilic microenvironments in the thallus.
- Bacterial microbiota correlated significantly with temperature and nutrients.
- Key bacteria might play relevant roles in adaptive responses of coralline algae.

GRAPHICAL ABSTRACT
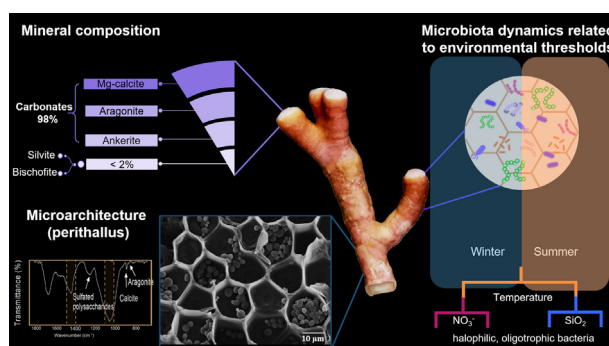
ARTICLE INFO

ABSTRACT

Coralline algae are worldwide carbonate builders, considered to be foundational species and biodiversity hotspots. Coralline habitats face increasing pressure from human activities and effects related to Global Change, yet their ecological properties and adaptive responses remain poorly understood. The relationships of the algal microbiota with the mineral bioconstructions, as well as plasticity and resilience of coralline holobionts in a changing environment, are of particular interest. In the Gulf of California, *Neogoniolithon trichotomum* (Rhodophyta) is the main carbonate builder in tidal pools. We performed a multi-disciplinary assessment of the *N. trichotomum* microstructure using XRD, SEM microscopy and SR-FTIR spectromicroscopy. In the algal perithallus, magnesium-calcite and aragonite were spatially segregated and embedded in a polysaccharide matrix (rich in sulfated polysaccharides). Mg-calcites (18–19 mol% Mg) were the main mineral components of the thallus overall, followed by iron carbonates related to dolomite (ankerite) and siderite. Minerals of late evaporitic sequences (sylvite and bischofite) were also present, suggesting potential halophilic microenvironments within the algal thalli. The diverse set of abundant halophilic, halotolerant and oligotrophic taxa, whose abundance increase in the summer, further suggests this condition. We created an integrated model, based on environmental parameters and the microbiota distribution, that identified temperature and nutrient availability

---

* Corresponding author.
  E-mail address: ablanco@uabcs.mx (A. Blanco-Jarvio).
[1] Denotes equal contribution.

(particularly nitrate and silicate) as the main parameters related to specific taxa patterns. Among these, *Hahella, Granulossicoccus, Ferrimonas,* Spongiibacteraceae and cyanobacterial Xenococcaceae and Nostocaceae change significantly between seasons. These bacterial components might play relevant roles in algal plasticity and adaptive responses to a changing environment. This study contributes to the understanding of the interplay of the prokaryotic microbiota with the mineral microenvironments of coralline algae. Because of their carbonates with potential resistance to dissolution in a higher pCO_2 world and their seasonally dynamic bacteria, coralline algae are relevant targets to study coastal resilience and carbonated systems responses to changing environments.

1. Introduction

Coralline habitats are main carbonate builders of coastal environments facing major transformations due to increasing human activities. Pollution, ocean warming and acidification are among the most recognizable threats for these biodiverse ecosystems (Nelson, 2009; Hofmann et al., 2014; Cornwall et al., 2019). Understanding the drivers of their diversity, dynamics and resilience are current challenges in the countdown of biodiversity loss related to Global Change. Diversity and dynamics of biomineralizing holobionts such as corals, sponges or coralline algae (CA) might provide relevant information to understand the building or losing potential of massive mineral bio-constructions, that ultimately model coastal morphology. Thus, CA and their associated microbiota are emergent targets to study the ecology of coralline habitats and coastal resilience, carbon cycling and ocean acidification. CA complex diversification and evolutionary history are revealed by the ability of this group to colonize a wide range of environmental conditions (e.g., high irradiance, high desiccation, oligotrophic conditions; Hofmann et al., 2018), enabling CA to remain a key component of benthic marine communities over geologic time (Aguirre et al., 2000). Much is known about coralline algae ecology and physiology, but a major focus is needed towards a new understanding of their responses to environmental changes (e.g., McCoy and Kamenos, 2015). While CA are recognized as biodiverse reservoirs and key coastal carbonate builders, it is particularly challenging to understand how carbonate structures harbor microbial life and how CA impacts microbial microhabitats. Previous studies have targeted morphogenesis associated with carbonated algal thalli (e.g., Cabioch, 1988; Foster, 2001). More recently, the microbiota and some features of the metabolism of rhodoliths (*Sporolithon austral*) have been studied from metagenomics-based metabolic profiles (Cavalcanti et al. 2014 and 2018). However, few studies have investigated biomineralization-associated structures and their relationship with CA microbiota.

Like in corals, both the vulnerability and resilience of CA depend on their association with symbiotic microorganisms (Reyes-Nivia et al., 2014). Some recent research is moving forward to describe the healthy microbiota and the pathobiome of CA. The models studied are different species of the genus *Neogoniolithon*: *N. fosliei* (Webster et al., 2011), *N. mamillare* (Meistertzheim et al., 2017) *and N. brassica-florida* (Quéré et al., 2019). Following different strategies, these experiments identified temperature-dependent changes of specific bacterial taxa (i.e., Proteobacteria and Bacteroidetes). Yet, microbiota specific function and its responses to environmental change are generally poorly understood.

Of the studies that do investigate biomineralization, several relate the vulnerability of coralline algae to its mineral composition. These studies mainly investigate the role of magnesium calcite (such as in *Lithothamnion muelleri*, McCoy and Kamenos, 2015), because it is known that magnesium minerals are overall more soluble than calcium ones. Relative solubility is critical for understanding the responses to ocean acidification. Recent studies regarding these topics are revealing algal (holobiontic) adaptation strategies to ocean acidification are diverse and complex, e.g. the resistance of the coralline rhodophyta *Jania rubens* to low pH/high pCO_2 was recently reported (Porzio et al., 2018), highlighting the potential of mineralization in algal physiology.

Nash et al. (2013) reported that high Mg content carbonates found in CA have higher resistance to dissolution than low Mg-calcites.

Calcarean algal microstructure has been studied with scanning electron microscopy (SEM) revealing biomineralizations with complex microstructure (Nash et al., 2019), but only few studies have reported experimental protocols that interlink microbial diversity with algal micro-environments. Although their interpretation is often complex, this kind of studies identify holobiontic responses to changing environmental conditions. Perkins et al. (2016) used high resolution hyperspectral fluorescence to identify an epiphyte micro-spatial gradient along the algal thallus, potentially linked to either pigment variation, light gradient, or nutrient availability. Fredericq et al. (2019) used cryo-SEM microscopy to provide clues to understand the algal inner allocation of floridean starch. X-ray microscopy, SEM-EDS and microtomography have also contributed to detect taxonomic features at microscale, including apical cells morphology and conceptacle characteristics (Krayesky-Self et al., 2016). Nash and Adey (2018) used novel protocols with SEM-EDS and field emission scanning electron microscope (FESEM) to describe Mg content differences between internal cell-wall and perithallus Mg content (in calcites), in a pioneer attempt to find the mechanisms that control rhodophyta biominerals diversity (see also Nash et al., 2013).

In this study, SEM microscopy, SR-FTIR spectromicroscopy and mineral determinations by X-ray diffraction (XRD and Rietveld refinement) are used to explore the microenvironments where algae and microbes interact. To explore the interplay of the prokaryotic communities with algal mineral bioconstructions, this study also builds a mechanistic model where *Neogoniolithon trichotomum* (coralline Rhodophyta) experienced the seasonality of tropical tidal pools. This seasonality is considered in a statistical model to select the environmental thresholds associated with prokaryotic abundance. Tidal pools prokaryotic bacterioplankton is analysed to distinguish the prokaryote patterns related to the algae.

2. Materials and methods

2.1. Sample collection

The tidal pools we studied are located in Calerita beach (Fig. 1) in La Paz Bay, in the West coast of the Baja California Peninsula. Sampling collections were conducted in February (winter) and September (summer) of 2018 at two tidal pools (Pool 1: 24°35′34.58″N, 110°28′ 34.43″W and Pool 2: 24°35′35.33″N, 110°28′35.33″W) of Playa Calerita, La Paz Bay, Mexico) (Fig. 1A). These pools have a maximum depth of ~0.3 m, and the alga *N. trichotomum* has the highest benthic cover (Hinojosa-Arango and Riosmena-Rodríguez, 2004; Kato et al., 2013). *N. trichotomum* is also a relevant carbonate builder of the region (Cruz-Ayala et al., 2001; Riosmena-Rodríguez et al., 2012). Physicochemical characterization of water surrounding coralline algae included temperature, pH, and conductivity (using a multiparametric Seabird probe). For both sampling efforts, triplicate water samples (30 ml each) were sequentially filtered through 0.45 and 0.22 μm nitrocellulose membranes and immediately frozen. Nutrient determinations of ammonium (here referred as $N-NH_4^+$), nitrate ($N-NO_3^-$), nitrite ($N-NO_2^-$), soluble reactive phosphorus ($P-PO_4^{-3}$) and soluble reactive silicon
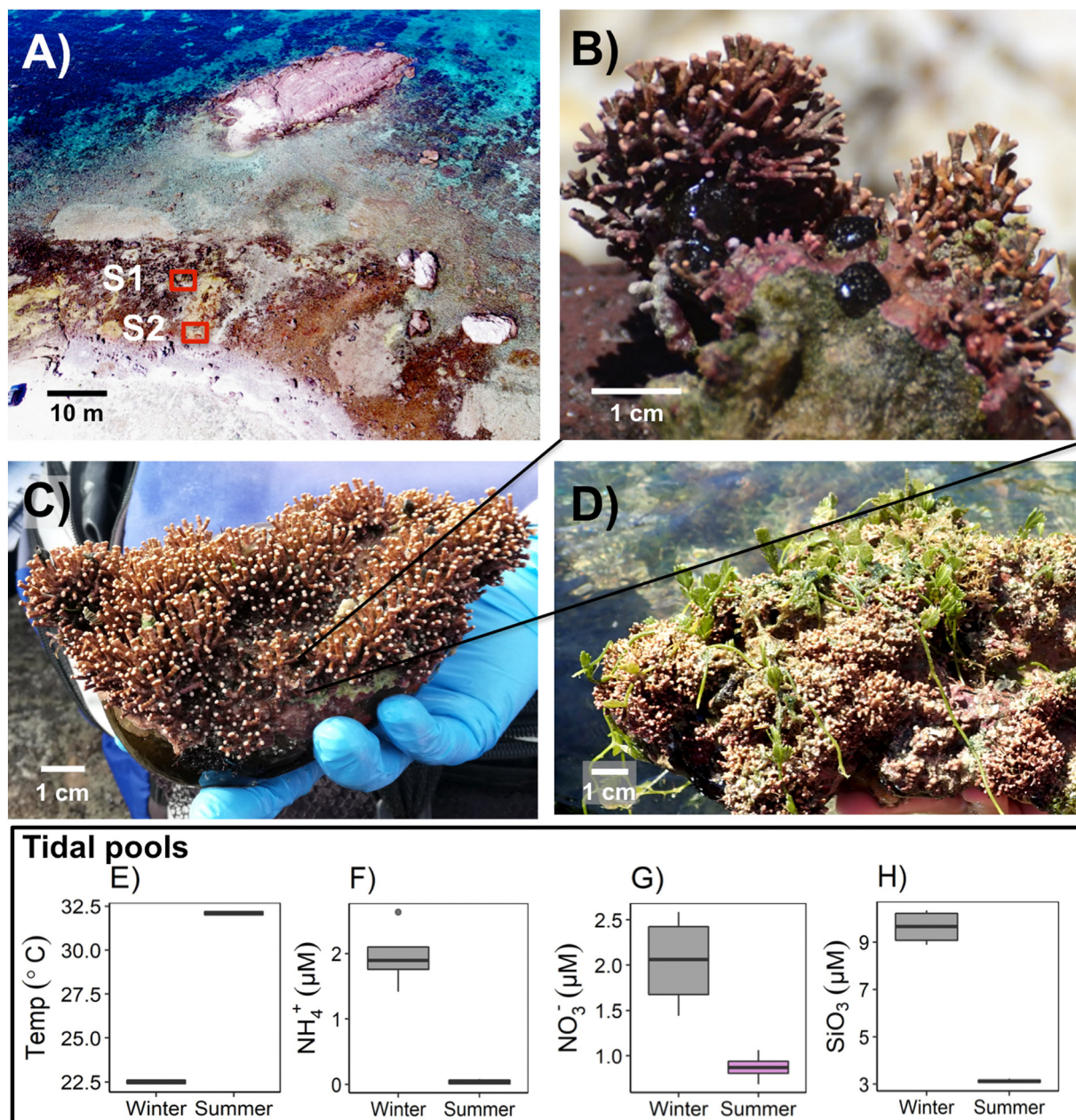
Fig. 1. (A) Calerita Beach, La Paz Bay, Mexico, boxes show tidal pools (Sites Sl and S2). *N. trichotomum* coralline Rhodophyta (B) thallus of approximately 3×3 cm, during winter (C) and summer (D) campaigns, when green algae *Caulerpa* sp. can be observed on the surface of *N. thricothomum*. E,F,G and H show physicochemical conditions (from left to right, water temperature, ammonium, nitrate and silicate concentration at depth < 1 m) of the tidal pools (average of two collection sites, $n = 6$) for winter and summer campaigns. (For interpretation of the references to colour in this figure legend, the reader is referred to the web version of this article.)

(Si-SiO$_2$) were carried out using a Skalar San Plus continuous-flow autoanalyzer (Kirkwood, 1994; Grasshoff et al., 1999) at the Aquatic Biogeochemistry Lab, UNAM, Mexico (whose expertise include low-nutrient aquatic environments (e.g., Planas et al., 1999; Coria-Monter et al., 2017). Unfiltered 10 ml water samples were used for total nitrogen (TN) and phosphorus (TP) determinations following the protocol reported by Valderrama (1981).

The sample nomenclature sample type-site-time was used to identify Rhodophyta algae (Alga = A) and water (Water = W), tidal pool (site 1 = S1, site 2 = S2) and collection time (winter = T1, summer = T2).

2.2. Preparation of samples for downstream analyses

Approximately 15 g of coralline algae were collected at <1 m depth (triplicates per pool, per season; total $n = 12$) and subsampled as follows. Each coralline algae thallus was manually cleaned out of macroscopic epibionts (using a stereoscopic microscope) and homogeneously divided into the next fractions: a) *Dried, pulverized subsamples* comprised: 4 g for XRD ($n = 3$ per sample) and 6 g for elemental analyses (n = 3 per sample), including organic nitrogen and phosphorus (N$_{org}$ and P$_{org}$) determinations. Persulfate oxidation of triplicate thalli pulverized and homogenized was performed following Valderrama (1981) and using a continuous flow Skalar San Plus autoanalyzer. b) *Dried intact surface:* for SEM microscopy, surface samples (n = 3 branches of ~1 mm of diameter) were cold-dried (< 40 °C) and their surface structure was preserved (this accounted for less than 1 g per sample). Samples for SEM were mounted on aluminum stubs with double sided carbon tape and gold-coated using a sputter coater Denton Vacuum Desk II. The specimens were examined and photographed with a JEOL JSM 5310LV scanning electron microscopy. c) *Frozen samples*: less than

<2 g per sample were placed into three separated vials and used for DNA extraction. d) *Fresh samples*: approximately 1 g (subsampled into n = 3 separated vials) were kept fresh for infrared spectromicroscopy (SR-FTIR) analyses (detailed methods are explained in Section 2.2.2).

2.2.1. Mineral characterization (XRD and Rietveld refinement)

For X-Ray Diffraction (XRD) analyses, whole rhodophyta thalli were cleaned with a brush, cold dried (<50 °C), ground, sieved (<45 μm) and homogenized using a pestle and agate mortar. Samples were mounted using double-side aluminum holders (as random fractions). XRD measurements were performed in an angular range 2θ from 5° to 90° with a step scan of 0.003° (2 Theta) and 40 s of integration time per step. Resulting diffractograms were obtained using an EMPYREAN diffractometer equipped with a Ni filter, copper tube, and a PIXCel 3D detector (at LANGEM, UNAM, Mexico).

Phase identification was made with PDF-2 and ICSD databases. Rietveld refinement of the data was done with the Highscore v4.5 software using a pseudo-Voig profile function. Some specimen-dependent parameters were refined, including the zero and displacement errors, polynomial fitting for the background, peak position, peak areas, scale factors, atomic coordinates, and preferred orientation. Weighted R profile (Rwp) and Goodness of fit (GOF) discrepancy indices were calculated. Mg in calcite was determined using XRD measurement and Rietveld refinement method (Rietveld, 1969) by calculation of lattice parameters (Titschack et al., 2011).

2.2.2. Synchrotron-based Fourier Transform Infrared spectromicroscopy (SR-FTIR) and data analysis

SR-FTIR is a label-free, non-invasive microprobe technique that has been used to obtain chemical information maps of biogeochemical samples with microscale spatial resolution (Holman et al., 1999; Probst et al., 2013; Valdespino-Castillo et al., 2018). The label-free SR-FTIR spectromicroscopy was used to obtain chemical information of Rhodophyta samples. Branches of freshly harvested samples were studied with SR-FTIR within seven days after collection. They were maintained in wet chambers that provided close-to -natural conditions of daily natural illumination, similar pH and salinity. Agitation was used to prevent anoxia. Immediately before SR-FTIR experiments, a thin film of *N. trichotomum* (epithallus and perithallus) were carefully dissected (using a stereoscopic microscope), "lifted" and, at room temperature, gently dried over a liquid nitrogen gas-flow, onto 1-mm thick ZnSe infrared crystals. Although drying affects the 3-dimensional structure of the thin samples, prior microscopy experiments with other similar samples suggest that the 2-dimensional structure is largely unaffected. Therefore, the measured spatial distribution of biogeochemical features likely represents their native 2-dimensional distribution within the sample. All SR-FTIR spectromicroscopy measurements were performed in the transmittance mode at the infrared beamline of the Advanced Light Source (http://infrared.als.lbl.gov/), where mid-infrared photons emitted from the synchrotron were focused with a 0.65 numerical aperture objective in a Nicolet Nic-Plan infrared microscope. Each spectrum was the average of 8 scans, with a spectral resolution of 4 cm^{-1}. Background spectra were obtained on the cell-free area of the crystal.

Spectra were collected in the mid-infrared region (~ 2.5 to ~15.5 μm wavelength, or ~ 4000 to ~650 wavenumber in cm^{-1}) at a spectral resolution of 4 cm^{-1} with 8 co-added scans and a peak position accuracy of 0.01 cm^{-1}. For each SR-FTIR imaging measurement, the entire view-field of the intact coralline mineralization was divided into equal-sized 2-μm × 2-μm squares before scanning. Background spectra were acquired from locations without coralline material and were used as reference spectra. A data cube of position-associated infrared spectra was obtained following each SR-FTIR data acquisition experiment. Software Thermo Electron's Omnic version 7.3. was used for data analyses. The absorption spectra were then subjected to preprocessing, baselines correction, and univariate image analysis. The univariate approach, which integrates infrared absorbance of an individual peak of interest, relates the absorbance intensity to the relative concentration of a particular chemical component through the Beer-Lambert Law, then generates a spatial map with pixel colour corresponding to peak area.

2.2.3. Total DNA purification and 16S rRNA gene amplification

To study prokaryote community composition, three organisms per pool were selected in the field (in winter and summer, total n = 12), samples included the basal, intermediate and apical parts of the thallus. Approximately 0.25 g from this fresh coralline algae composite sample were used for triplicate total DNA extraction using the DNeasy PowerSoil® kit (Qiagen) according to the manufacturer's instructions. To distinguish prokaryotic communities associated to algae from those associated to the water of the pools, we purified total DNA samples of the water surrounding coralline algae (two samples per pool, per season, total n = 8) were obtained by filtering 500 ml of pool-water through 0.22 μm cellulose acetate free membranes (ThermoFisher Scientific®). These filters were kept in liquid nitrogen until DNA extraction, which was performed with the PowerWater® kit (Qiagen) according to the manufacturer's instructions. The DNA obtained was quantified by fluorometry, using the QubitTM 4 Fluorometer kit (ThermoFisher Scientific) and stored at −20 °C until analysis.

The hypervariable V4 region of the 16S rRNA gene was amplified from total DNA (in triplicates per sampling site) by PCR using the primers 515F/806R (Caporaso et al., 2010; Caporaso et al., 2012), PCR reactions contained a specific Golay in the reverse primer (Caporaso et al., 2010). PCR reactions plus negative controls were prepared with nuclease-free water and 2 ng/μl of total DNA per sample. Every PCR mix of a final volume of 25 μl contained 2.5 μl Takara ExTaq PCR 10× buffer (1× final concentration) (TaKaRa Corp., Shiga, Japan), forward and reverse primers (10 μM final concentration), 2 μl of Takara dNTP mix (2.5 mM), 0.75 μl MgCl2 25 mM (0.75 mM final concentration) and 0.625 U Takara Ex Taq DNA Polymerase. The amplification program included a (94 °C, 1 min) initial denaturalization step followed by 35 cycles of 94 °C (30 s) - 55 °C (30 s) - 72 °C (30 s), and a final (72 °C, 10 min) extension. When no amplicons were detected in the negative controls, the PCR products from three PCR reactions were pooled and purified for each tidal pool (~20 ng per sample). Purification was done with the Agencourt AMPure XP PCR Purification system (Agencourt Bioscience Co.) and the SPRI platform (Beckman Coulter, Brea, CA, USA). Sequences were obtained on an Illumina MiSeq platform (Yale Center for Genome Analysis, CT, USA), resulting in ~250bp paired-end reads. Sequences were deposited in GenBank under BioProject PRJNA643495. BioSample metadata are available in the NCBI BioSample database (http://www.ncbi.nlm.nih.gov/biosample/) under accession numbers SAMN15415156 (Algae.s1.t1), SAMN15415157 (Algae.s1.t2), SAMN15415158 (Algae.s2.t1), SAMN15415159 (Algae.s2.t2), SAMN15415160 (Water.s1.t1), SAMN15415161 (Water.s1.t2), SAMN15415162 (Water.s2.t1) and SAMN15415163 (Water.s2.t2).

2.2.4. Sequence analyses

The 16S rRNA gene sequences obtained were analysed with QIIME2 (Bolyen et al., 2019). Sequences were demultiplexed and filtered to remove low-quality sequences, chimerae, and singletons using DADA2 (Callahan et al., 2016) algorithms. This pipeline allowed us to obtain Amplicon Sequence Variants (ASV). Relative abundance of ASVs per sample can be consulted in Supplementary Fig. S1; PCoA ordination of ASVs using Bray-Curtis distance and shared ASVs among groups is visualized in Fig. 4. Rarefaction analysis was performed using a diversity alpha-rarefaction visualizer, at a sampling depth of 6900 sequences per sample, where accumulation curves were asymptotic for each case. Taxonomic classification was done using the 'q2-feature-classifier' plugin (https://github.com/qiime2/q2-taxa) based on the SILVA database (http://www.silva-arb.de). Details about the number of sequences per sample can be consulted in Supplementary Table S2.

P.M. Valdespino-Castillo, A. Bautista-García, F. Favoretto et al.

Science of the Total Environment 757 (2021) 143877

Table 1

Physicochemical parameters of the water environment of study sites (Pool 1 and Pool 2) in Calerita, La Paz Bay in the winter and summer of 2018. Additionally, algal biomass organic nitrogen and phosphorus content.

	Winter		Summer		Kruskal-Wallis
	Site 1	Site 2	Site 1	Site 2	
Temperature (°C)	22.6	22.4	32.2	32	*
pH	8.63	8.64	8.54	8.57	
Salinity (psu)	35	35	35	35	
Irradiance (LUX)	16,779	16,749	55,341	52,642	
NH_4^+	2.15 ± 0.24	1.57 ± 0.14	0.06 ± 0.03	0.03 ± 0.02	*
NO_3^-	1.56 ± 0.09	2.40 ± 0.10	0.79 ± 0.05	0.87 ± 0.11	*
NO_2^-	0.26 ± 0.008	0.22 ± 0.01	0.03 ± 0.002	0.03 ± 0.003	*
$P\text{-}PO_4^{-3}$	3.08 ± 0.07	0.66 ± 0.58	0.28 ± 0.01	0.24 ± 0.03	*
$Si\text{-}SiO_2$	9.26 ± 0.01	9.24 ± 0.46	3.14 ± 0.05	2.85 ± 0.22	*
DIN	3.96 ± 0.35	4.19 ± 0.25	0.89 ± 0.08	0.93 ± 0.14	*
$DIN{:}P\text{-}PO_4^{-3}$	1 ± 0.23	6 ± 0.21	3 ± 0.39	4 ± 0.25	
TN	33.31 ± 2.65	23.4 ± 1.11	44.1 ± 3.95	38.94 ± 4.28	
TP	7.84 ± 0.08	1.23 ± 0.04	1.70 ± 0.13	1.39 ± 0.17	*
TN:TP	4 ± 0.29	19 ± 0.29	26 ± 2.81	28 ± 0.49	*
Biomass					
N_{org}	46.74 ± 0.34	36.45 ± 1.51	12.95 ± 1.14	6.28 ± 0.83	*
P_{org}	92.31 ± 1.90	105.17 ± 10.37	70.92 ± 0.78	78.25 ± 0.52	*
$N_{org}{:}P_{org}$	0.51 ± 0.01	0.35 ± 0.04	0.18 ± 0.01	0.08 ± 0.01	*

* Kruskal-Wallis significance test ($p < 0.05$).

2.2.5. Statistical analysis

Univariate comparisons of environmental variables were made using Kruskal Wallis tests to study differences between summer and winter. Then, the ASV abundance from water and algae samples was scaled by dividing the centered columns by their standard deviations, and a Pearson distance metric was calculated and plotted for each taxon in a heatmap used for visualization. Taxa at the Family level with presence in at least 50% of the samples (abundance threshold >20 and showing complete taxonomic assignment at Family taxonomic level) were selected and ordered for visualization according to a fuzzy clustering with two a priori groups selected (k = 2, corresponding to Time 1 and 2) (Supplementary Fig. S2). To further explore the difference in ASV abundance among algae samples, we performed a non-Metric Multidimensional Scaling (nMDS) using Bray-Curtis distance (Fig. 5A). To determine statistically relevant environmental and physiological variables we used the envfit() algorithm (vegan package v. 2.5–6.) (Oksanen et al., 2019) in the R programming environment (R Core Team, 2019; R Studio Team, 2019). We explored the relationship between the selected ASVs and the environmental variables by using a Multivariate Regression Tree technique (MRT) (Fig. 6). MRT is a constrained clustering technique

Table 2

Non-Metric Multidimensional Scaling (nMDS) using Bray-Curtis distance among prokaryotic communities of algal samples. Statistical significance (asterisks) of environmental variables related to prokaryote samples was obtained by using the envfit() algorithm.

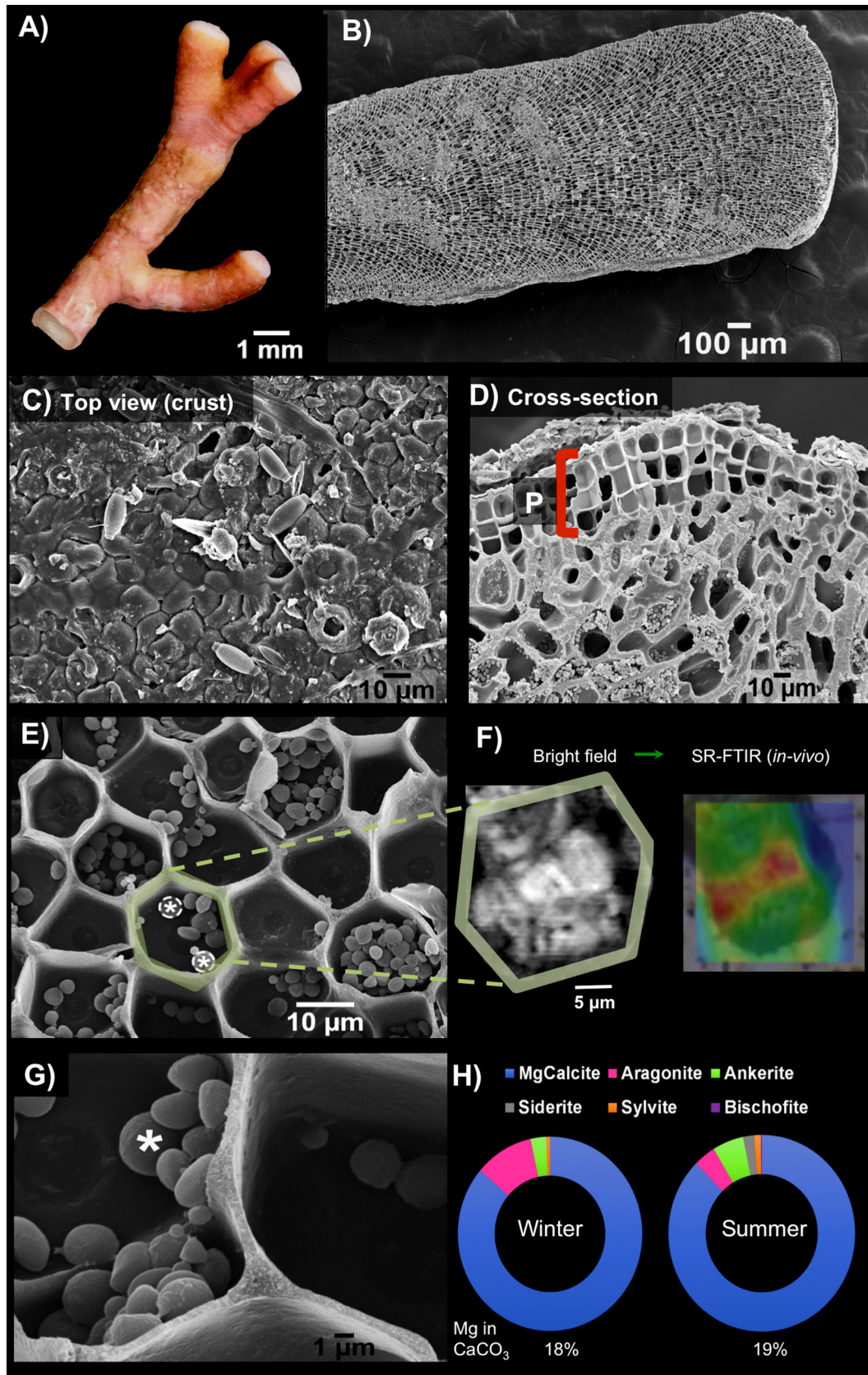| Variables	NMDS1	NMDS2	r2	Pr(>r)	
Temperature	0.95522	0.2959	0.8904	0.0002	***
Irradiance	0.94723	0.32055	0.8853	0.0007	***
$N\text{-}NH_4^+$	-1	−0.0093	0.7738	0.0039	**
$N\text{-}NO_3^-$	−0.9697	−0.2445	0.8109	0.0002	***
$N\text{-}NO_2^-$	−0.9817	−0.1903	0.8331	0.0016	**
$P\text{-}PO_4^{-3}$	−0.9996	0.02826	0.2955	0.1935	
$Si\text{-}SiO_2$	−0.9899	−0.142	0.8196	0.0016	**
DIN	−0.9935	−0.1141	0.8867	0.0004	***
$DIN{:}PO_4^{-3}$	−0.35	−0.9367	0.0724	0.7179	
TP	−0.9616	0.27435	0.1627	0.3894	
TN	0.94582	0.32468	0.5487	0.0251	*
TN:TP	0.94274	−0.3335	0.5373	0.0351	*
DIN:TP	−0.8624	−0.5062	0.4331	0.0879	.
$P_{org\text{-}biomass}$	0.56041	0.82822	0.2612	0.2495	
$N_{org\text{-}biomass}$	−0.2834	0.95901	0.0893	0.6703	
$N_{org}{:}P_{org}$	−0.5585	0.8295	0.1244	0.5614	

(De'Ath, 2002), which allows the partitioning of a quantitative response matrix by a matrix of explanatory variables constraining on where to divide the data of the response matrix. Similarly to a Redundancy Analysis (RDA), MRT performs better for highlighting local structures and interactions among variables. An advantage of MRT is that it does not make any assumptions on the shape of the data distribution and it is robust in the presence of missing values and collinearity. The MRT techniques split the data into clusters of samples, similar in their species compositions, based on threshold values (environmental variables in this case). We performed the analysis using the function mvpart() from the package mvpart (Therneau and Atkinson, 2014) that computes both the partition and the cross-validation of the tree. The cross-validation identifies the best predictive tree and is measured by the cross validated error (CVRE) that tends to maximize the overall R^2. Further detail on the theory behind the method can be found in De'ath (2002). Data and code related to the results can be consulted at https://github.com/Fabbiologia/Coralline-algae-habitats.

3. Results

3.1. Physicochemical environments of the tidal pools

The physicochemical variables measured at each sampling site are shown in Table 1. Physicochemical parameters measured evidenced an oligo-to-mesotrophic habitat in both pools. Salinity and pH were relatively stable between seasons (summer and winter), temperature and irradiance were higher in the summertime, and representative overall of the regional conditions (Salinas-González et al., 2003). Regarding nutrient content, statistically significant differences between seasons were found for the three N inorganic species, for $P\text{-}PO_4^{3-}$ and for TP. Phosphorus content was more heterogeneous than nitrogen in the pools (Table 1). Besides the change in the nutrient status of the pools (more availability of N and P during the winter), a relevant difference between the seasons was the growth of green algae during the summer, when *Caulerpa* sp. colonized large areas of the pools (BICA survey 2018, unpublished), on the surface of *N. trichotomum*.

Thallus biomass N_{org}, P_{org}, as well as the $N_{org}{:}P_{org}$ ratio showed statistically significant differences (marked with asterisks) between seasons (Table 1). $N_{org}{:}P_{org}$ averaged 0.43 (T1) and 0.13 (T2), being two orders of magnitude smaller than 16 (N:P Redfield ratio), suggesting nitrogen limitation. Interestingly, this signal was generalized and did not follow the local variation of the surrounding water, where –as explained

P.M. Valdespino-Castillo, A. Bautista-García, F. Favoretto et al.

Science of the Total Environment 757 (2021) 143877

Fig. 2. Mineral composition and microstructure of *N. trichotomum*. A) *N. trichotomum* thallus branch. SEM microscopy of B) branch longitudinal section, C) intact surface showing epibiontic diatom frustules, D) Cross-section (i.e., lateral view) profiling of thallus showing perithallus cells (P), E, G) Perithallus cells close-up showing spherical endolithic structures (usually referred as Floridean starch, asterisk) and carbonated cell walls. (F) Bright field microscopy of fresh perithallus cells (used for SR-FTIRs in vivo analyses). H) Mineral composition (as percentage) determined by XRD and Rietveld method from dried pulverized algal thalli from winter and summer.

before– phosphorus was more abundant in site 1, driving heterogeneity in DIN:P-PO$_4$ and TN:TP ratios.

3.2. Microstructural analyses

3.2.1. Microarchitecture and mineral composition

The microstructure of *N. trichotomum* thallus is complex; some features of the carbonated structure are depicted in Fig. 2 at different scales. Epibionts such as diatoms (frustules) were visualized on the intact surface of *N. trichotomum* using SEM microscopy (Fig. 2C). The top surface view (Fig. 2C) shows cell facets of a relatively regular geometry, resembling a hexagonal shape (cell diameter ~ 15 to 20 μm) assembled on an approximately flat surface. A cross-section (lateral view, Fig. 2D) was helpful to reveal an external flat structure as thick as ~3–7 μm that covers the branch surface and inner structures. The perithallus is characterized by three layers of apical cells (Fig. 2D) followed by multiple layers characterized by a thicker mineral structure of irregular shapes (hypothallus anastomoses sensu Cabioch, 1988, resembling deformed or bent caveats). The inner walls and interfilament walls of hypothallus are ~2 μm thick, contrasting with thin (~0.6 μm) walls separating apical cells (Fig. 2D, E). Round structures of ~1 μm or less in diameter are found in the interior of the perithallus and the hypothallus. Heterogeneous, segregated bulky materials in a perithallus cell were visualized using bright field microscopy and SR-FTIR spectromicroscopy (Figs. 2F and 3).

The XRD mineral composition of winter and summer samples is shown in Fig. 2H. Carbonates (aragonite, Mg-calcite, ankerite and siderite) represent close to 98% of the total mineral content. Magnesium-calcite ranged from 83 to 90%, aragonite from 3 to 12% and the sum of ankerite and siderite (carbonates enriched in iron) from 1 to 10% (in weight). Sylvite contributed between 0.5 and 2% in weight and was found in all samples. Bischofite was detected in low proportion (<1% in weight) only in samples of pool 2, during summer. The magnesium content of calcite was slightly different for samples collected in winter

(18% mol of MgCO$_3$) and summer (19% mol of MgCO$_3$) as calculated from the cell parameters (a, c, V) obtained from the refinement of mineral structures by the Rietveld method (Rietveld, 1969) and using the calibrations established by Titschack et al. (2011) (Section 2.2.1). Weighted R profile (Rwp) and Goodness of fit (GOF) discrepancy indices were calculated for all the samples between [4.9 to 6.3] and [0.57 to 0.72] respectively.
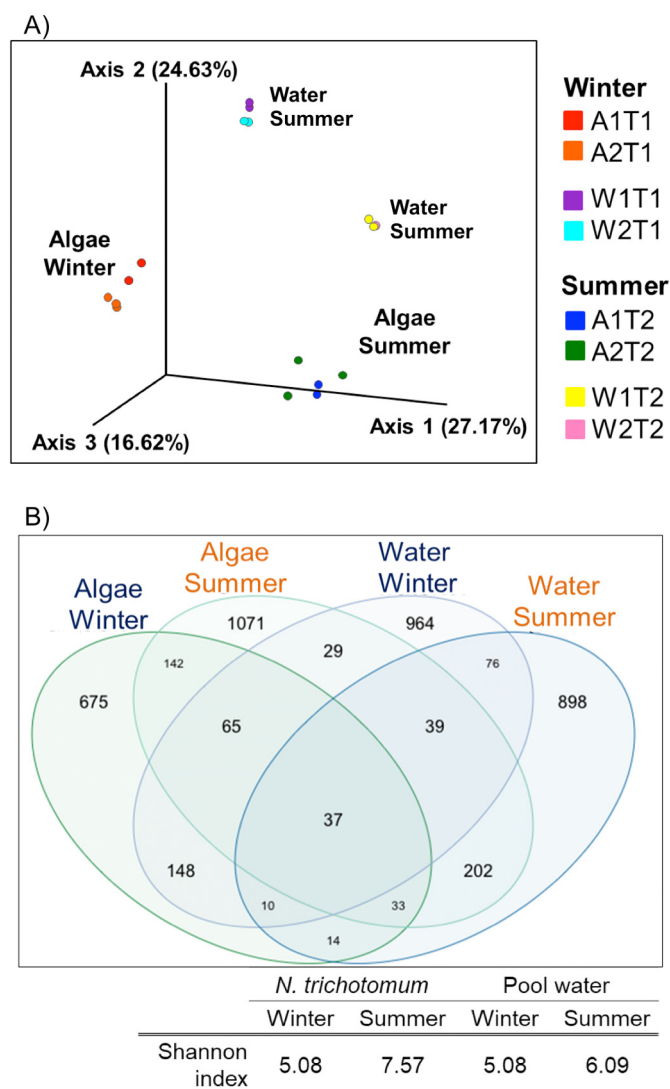
3.2.2. SR-FTIR microscopic probing of biomolecules and minerals in the living algal holobiont

We further conducted SR-FTIR spectral microscopic examinations of the intact epithallus (potential sloughing layer) of a summer *N. trichotomum* sample (Fig. 3A) which revealed infrared absorptions at ~1045 cm^{-1}, which are associated with polysaccharides (Higgins et al., 1961; Tipson and Cohen, 1968, see also references in Valdespino-Castillo et al., 2018 referred to biomineralizing microbial mats). We observed additional signals at ~1030, ~1114, and ~1626 cm^{-1}, which are associated with a surface rich in silicates and coordinated water in silicates, and at ~874 cm^{-1} and ~ 1416 cm^{-1}, which are associated with low-Mg calcite (Fig. 3A, infrared heat maps and spectra from location #1-#3). The polysaccharide absorption band arises from vibrations of atomic groups C—O, C—C, C-OH in polysaccharides. The absorption features of these silicates are well-described for the Si—O vibration modes in layer silicates and for Si-O-Si, O-Si-O vibration modes in 3-dimensional silicates (Farmer, 1975). The carbonate mineral absorption features described above are those well established for ν_3 (CO$_3$)$^{-2}$ and ν_3(CO$_3$)$^{-2}$ modes in Mg calcite (Andersen and Brecevic, 1991; Valdespino-Castillo et al., 2018; Stanienda-Pilecki, 2019). The less prominent absorption peaks observed at ~854 and ~ 1445 cm^{-1} are consistent with the reported low proportion of aragonite.

An examination of the spectral characteristics of the bare area (marked by a dotted circle in Fig. 3A) reveals additional absorptions at ~1540 and ~ 1640 cm^{-1} that are associated with amide II and amide I
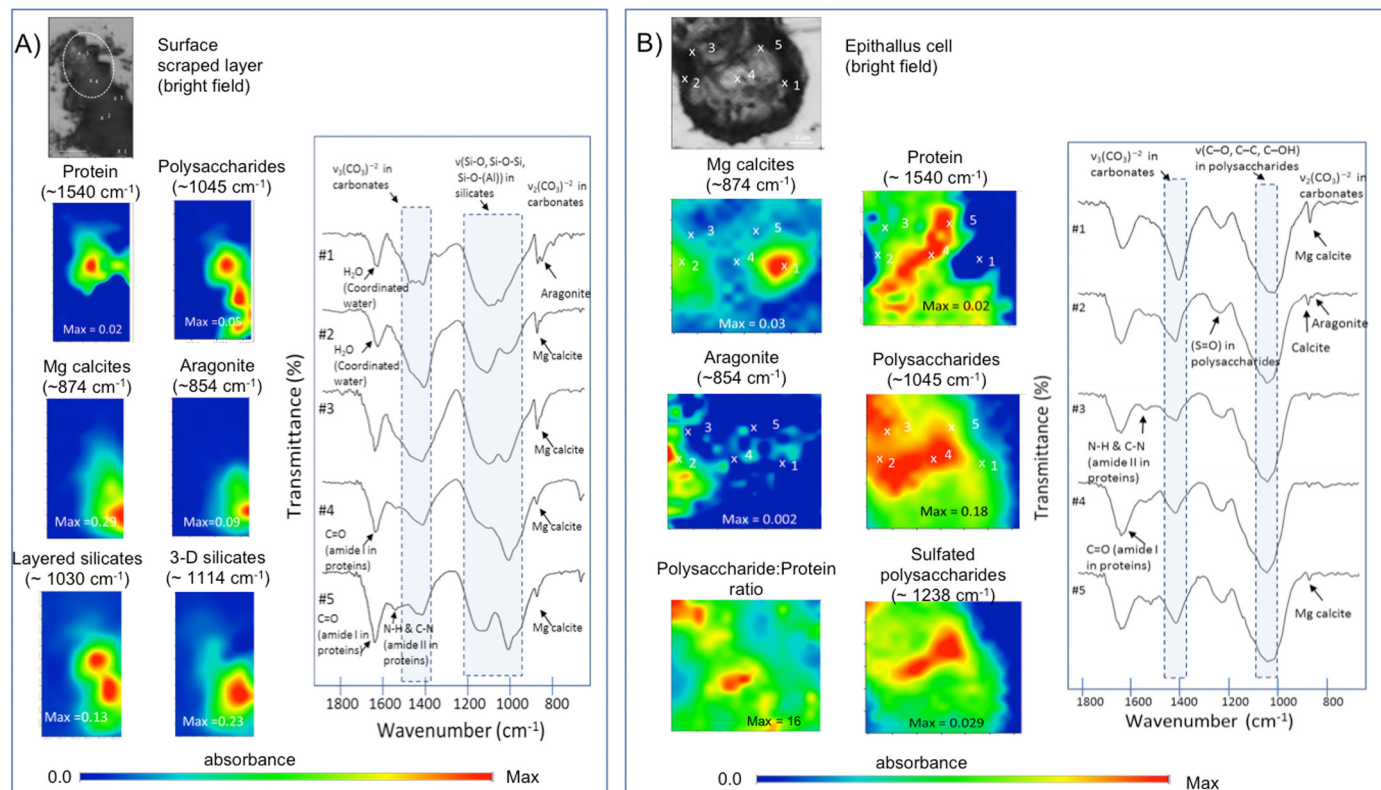
Fig. 3. SR-FTIR spectromicroscopy of fresh *N. trichotomum* surface (summer). A) epithallus (presumably sloughing) layer. Spatially resolved heatmaps of band assignment of structural minerals (Mg-calcite and aragonite) and carbohydrates of embedding organic matter of *N. trichotomum* perithallus. B) Distribution heat maps of the carbohydrates vibration modes at ~1000 cm^{-1}, calcite at ~870 cm^{-1}. Scale bars: 10 μm. Transmittance is given in % units.

A)

B)

	N. trichotomum		Pool water	
	Winter	Summer	Winter	Summer
Shannon index	5.08	7.57	5.08	6.09

Fig. 4. A) Principal coordinates analysis (PCoA) ordination plot based on the Bray-Curtis distance showing the similarity of prokaryotic community composition per sample type (including high similarity between pools) but showing larger differences between algal and water prokaryotic communities, and also between winter and summer (Alga = A, Water = W, Winter = T1 and Summer = T2). B) Representation of a Venn diagram considering bacterial amplicon sequence variants (ASVs) and average Shannon index of the four different groups visualized in the ordination.

vibrational modes in proteins, probably from diatoms (spectra recorded at locations #4 and #5).

For the perithallus cells, SR-FTIR spectromicroscopy reveals that the mineral structure of repeating hexagonal shapes in Fig. 2E, F is made out with carbonates including Mg calcite and aragonite (Fig. 3B). It also reveals that the bulky content located in the interior of perithallus cells is rich in sulfated polysaccharides (Fig. 3B).

3.3. Prokaryotic community composition

A total of 1,053,241 raw sequence reads were obtained (V4 hypervariable region of the 16S rRNA gene, ~290 bp) from Bacteria and Archaea domains. After quality controls, 506,767 sequences were recovered and analysed, 64% of which belonged to *N. trichotomum*

microbiota, and 36% to pool water microbiota. Sequences accounted for a total of 7622 ASVs; 4013 of them were related to *N. trichotomum* microbiota and 3609 to pool water microbiota. The microbial composition ordination using Bray-Curtis distance (PCoA) is depicted in Fig. 4. Four distinctive groups can be recognized, showing clear (distance) differences between algal and water microbiota, and between winter and summer samples. A representation of a Venn diagram (Fig. 4B) considering bacterial ASVs of the four different groups (algae-t1, algae-t2, water-t1 and water-t2) shows that only ~0.7% of total ASVs is shared among all groups. When analysed per sample type, the two different sets of algae shared 10.1% of ASVs and water groups shared 6.1%. When analysed by season, Winter groups shared 10.4% of ASVs and Summer groups shared 10.6%. These results were obtained after purifying DNA with different extraction kits: for water samples and for soil in the case of algae (following the protocols of Earth Microbiome Project), and this factor may influence the results.

At Domain level, Bacteria (99.8% of reads) dominated over Archaea (0.14%) within the entire dataset (algae and water samples). Archaeal taxa were mainly found in the water samples, and the most represented taxa included Parvarchaeota > Crenarchaeota/Thaumarchaeota and Euryarchaeota. Bacterial main groups were Proteobacteria > Bacteroidetes > Cyanobacteria (Supplementary Fig. S1). The most abundant phylum for both microbiota samples (*N. trichotomum* and water) was Proteobacteria, within this, Gammaproteobacteria and Alphaproteobacteria taxa had the highest abundance. Gammaproteobacterial Alteromonadales are overall abundant and displayed heterogeneity between samples (type and season) (Supplementary Fig. S1). Regarding Bacteroidetes, the most abundant classes were Flavobacteriia and Cytophagia (Supplementary Fig. S1). In the first case, the abundance was higher in the water than in algae during summer, but this pattern was the opposite during the winter. Cytophagia, instead, was more abundant during the summer in both water and algal samples. For Cyanobacteria, the most represented families were Oscillatoriophycideae (more abundant in the algal microbiota) and Synechococcophycideae (more abundant in pool-water during the summer). Differences among selected groups will be discussed further in the manuscript (in Section 4.3).

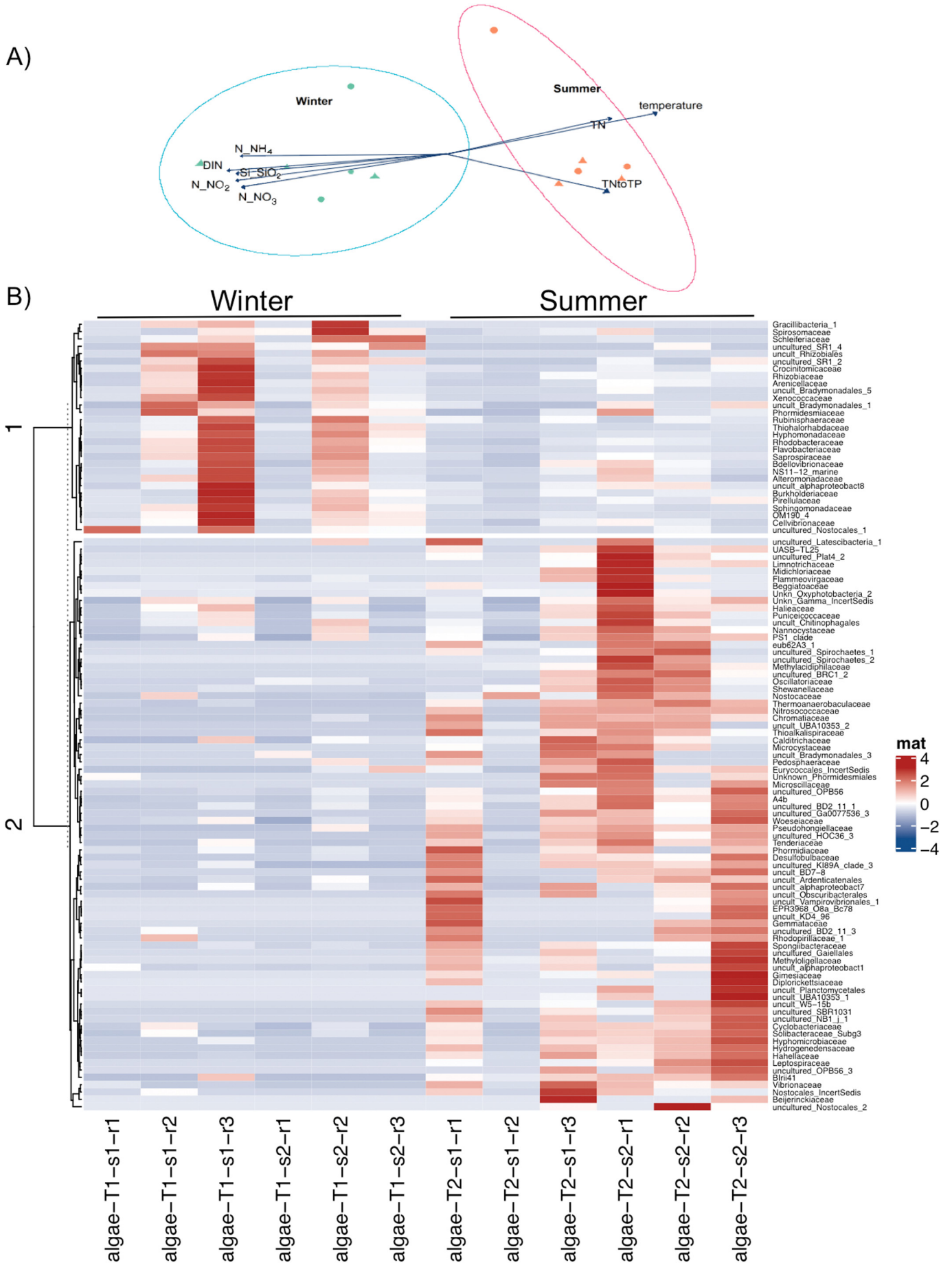### 3.3.1. Prokaryotic diversity in alga versus water samples

By comparing pool-water and algal samples, we determined a specific, distinctive prokaryotic microbiota of the algal holobiont. Our results show a) this microbial assembly is different from that of the surrounding water (Fig. 4), b) the community structure is overall similar at higher taxonomic ranks, but at deeper levels the differences accentuate (Supplementary Fig. S2), and c) the algal microbiota showed seasonal variation between the two periods explored (Fig. 5). Taxonomic units (ASV) counts and Shannon diversity index are shown in Fig. 4, illustrating that in both microbiota samples (algae and water) higher ASV counts and higher diversity are related to Time 2 (summer conditions). A similar Shannon index was shared by winter algal and water microbiota. The highest Shannon diversity index was found in the prokaryotic communities of alga samples collected during summer.

3.4. Correlation between prokaryotic community composition and environmental factors

Temperature, irradiance and nutrient content define (with statistical significance) winter and summer conditions at Calerita pools. Algal prokaryotic communities group according to these contrasting seasons (Figs. 4 and 5).

Fig. 5. A) nMDS analyses of algal prokaryotic communities in winter (blue) and summer (red). Circles correspond to samples of pool 1 and triangles, of pool 2. Arrows represent significant fitted environmental and physiological variables (Stress = 0.02; p-values can be consulted in Table 2). B) Relative abundance of microbial taxa at family level. Taxa with higher abundance in winter are grouped in the upper cluster, and taxa exhibiting more abundance in summer comprise the cluster beneath. (For interpretation of the references to colour in this figure legend, the reader is referred to the web version of this article.)

P.M. Valdespino-Castillo, A. Bautista-García, F. Favoretto et al.

Science of the Total Environment 757 (2021) 143877

Prokaryote families that showed higher abundance during winter included: Arenicellaceae, Xenococcaceae, Phormidesmiaceae, Alteromonadaceae, Bdellovibrionaceae, Burkholderiaceae, Sphingo monadaceae, Flavobacteriaceae, Rhodobacteraceae and Thiohalor habdaceae. Abundant bacterial families of the alga holobiont found during summer were Phormidiaceae, Nostocaceae, Oscillatoriaceae, Hahellaceae, Shewanellaceae, Spongiibacteraceae, Chromatiaceae, Planctomycetales, Gammaproteobacteria KI89A (symbionts of corals and sponges; Baquiran et al., 2020), and Pseudalteromonadaceae.

To find relationships between the environmental variables and the microbial distribution at the family level, a mechanistic model of algal microbiota was constructed (MRT model, Section 2.2.5). This was useful to detect the environmental thresholds with higher influence on microbial community composition (Fig. 6). Temperature was the variable with the highest explanation power, followed by two secondary nodes related to pool-water nitrate (N-NO$_3^-$, winter) and silicate (Si-SiO$_2$, summer) thresholds. The statistical scores of the taxa that better explain a significant portion (percentage of deviance) and the nodes of the MRT
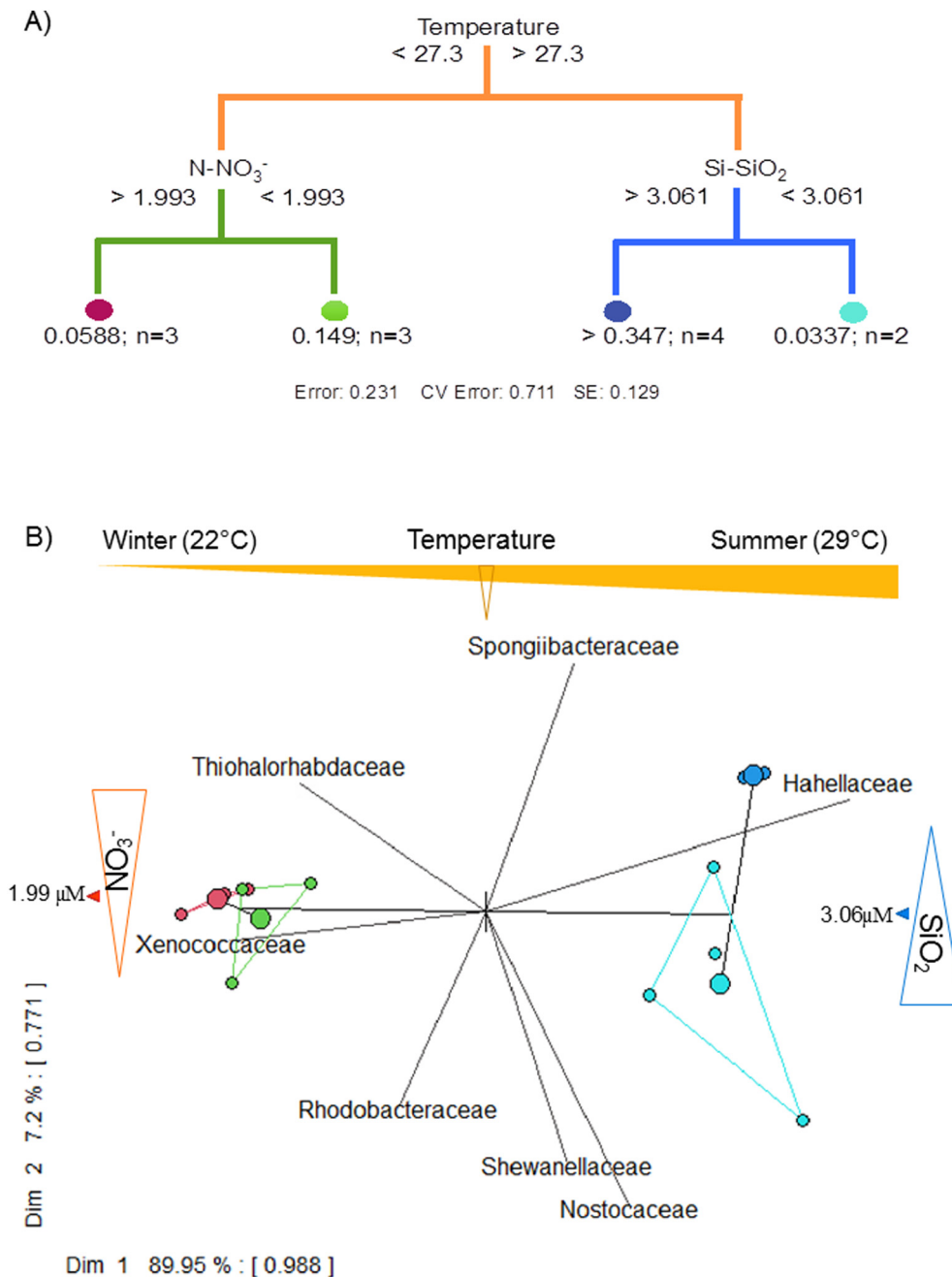
Fig. 6. A) MRT analyses showing the first separation of the clusters by a temperature threshold representing the two different seasons (see Table S2). MRT analyses, the first node of the model corresponds to temperature (explaining most of the variation; 89.95%). On a lower pruning of the tree, nitrate (N-NO$_3^-$) and silicate (Si-SiO$_2$) were the most important variables related to prokaryotic taxa patterns. The percentages of deviance of the bacterial families explaining most of the variation are summarized in Supplementary Table S1. The bacterial taxa related to environmental thresholds are depicted by the same colour in A and B (red >1.99 and green <1.99 μM of N-NO$_3^-$; violet >3.06 and cyan <3.06 μM of Si-SiO$_2$). Bacterial taxa are plotted in a two dimensional space by means of a Principal Component Analysis (PCA) in B), where colors of the larger points represent nodes (or centroids) of the clusters from the regression tree. The smaller points represent the samples within the cluster. Arrows and labels represent the most important microbial taxa characterizing the different cluster groups. (For interpretation of the references to colour in this figure legend, the reader is referred to the web version of this article.)

model are shown in Supplementary Table S1. The relative abundance (per sample) of the bacterial families with the higher scores (e.g., Xenococcaceae, Nostocaceae, Hahellaceae, Shewanellaceae, Thiohalorhabdaceae, Spongiibacteraceae and Rhodobacteraceae) at deeper taxonomic level (genus) is shown in Supplementary Fig. S3; where references of their previously reported halophilic, halotolerant and oligotrophic features can be consulted.

Among the bacterial genera exhibiting significant relationships with environmental thresholds, two stood out, exhibiting opposite patterns: *Hahella* (Hahellaceae), whose abundance drastically changed from winter (0.014–0.34%) to summer (5.1–19.8%) is related to the warmest, lower Si-SiO$_2$ region of the model. And *Granulosicoccus* (Thiohalorhabdaceae, with an abundance decreasing from winter (2.9–9.6%) to summer (0.13–0.48%) is related to the cooler, higher nutrient region of the model. Both genera were found in the two seasons, suggesting they might be components of the core microbiota of *N. trichotomum*. Temperature was related to 86% of the seasonal microbiota dynamics (Xenococcaceae and Hahellace patterns explained (each) >15% of the deviance of this main node). Xenococcaceae and Thialorhabdaceae patterns explained (each) > 10% of the secondary N-NO$_3^-$ node.

Nostocaceae and Spongiibacteraceae (mostly represented by BD1–7 clade microbes) explained (each) > 10% of deviance of the secondary Si-SiO$_2$ node (Fig. 6, Table S1). In the warmer, higher Si-SiO$_2$ region of the model, Nostocaceae comprises the cyanobacterial genera *Calhotrix, Cylindrospermopsis, Rivularia* and *Richelia* (Supplementary Fig. S3). Shewanellaceae is placed in a similar position to Nostocaceae in the model (the warmest and Si-SiO$_2$ oligotrophic). *Ferrimonas* (Shewanellaceae) exhibits a relative abundance of 0.16 to 1.5% during summer and is the dominant genus in the warmer, higher Si-SiO$_2$ region of the model (Fig. 6).

4. Discussion

Rhodophyta are some of the most intriguing and interesting organisms of coralline habitats because of their complex evolutionary history and their ability to colonize and tolerate life-challenging habitats (e.g., high irradiance, high desiccation, oligotrophic conditions). Our results show that some characteristics of their microbiota and their mineral microstructure might contribute to their plasticity and potentially, to adaptation and resilience to environmental changes. The results overall point to specific relationships of mineral microstructural features with prokaryotic patterns regarding carbonates and evaporite minerals: a) The mineral thallus of *N. trichotomum* is mainly composed by high Mg calcites. Ankerite (a mineral in the group of dolomites) was also found. These minerals potentially provide a higher strength to the algal carbonated structure compared to Mg-calcite, largely referred as the predominant mineral in coralline Rhodophyta. *Ferrimonas* (whose abundance increases in the summer) is a taxon suspected of contributing to iron accumulation, and potentially related to iron carbonates formation. Different *Ferrimonas* isolates have been described as halotolerant, halophilic and anaerobic (Katsuta et al., 2005). The phototrophic taxa potentially contributing to biomineralization through the photosynthesis engine include Xenococcaceae and Nostocaceae. b) The presence of evaporite minerals such as sylvite and bischofite suggests indirectly the existence of halophilic microenvironments in the algal thallus. This suggestion is concurrently supported by an important set of known halophilic bacteria detected (e.g., Hahellaceae) that increase its abundance in the summer (Section 4.2.3).

Although Calerita tidal pools exhibit conditions considered oligotrophic in both seasons, the physicochemical environment seems to be a major driver of prokaryotic community composition. Specific significant correlations of microbial taxa with environmental parameters structured a prokaryote microbiota model. In this, temperature and nutrient concentration (particularly nitrate and silicate availability) were identified as the factors that better explained algal prokaryotic microbiota

changes from winter to summer. The groups with the higher contribution to seasonal community change might be key to face environmental change in the coralline algae pools (Sections 4.3 and 4.4).

4.1. Tidal pools are oligotrophic habitats with seasonal variation

The aquatic environment of the tidal pools showed marked seasonality. Overall, pools showed lower temperature and higher nutrient contents during the winter that followed the natural marine conditions of La Paz Bay (Merino, 1987; Coria-Monter et al., 2017), where upwelling brings nutrients to surface waters during the winter. When compared to our light measurements, this pattern suggests a decoupled availability of light and nutrients (i.e., more availability of nutrients in winter vs. more light availability in the summer). In spite of a higher winter availability, the nutrient range within the tidal pools corresponded to oligotrophic habitats in both seasons. The phosphorus differences found between pools are consistent with the partial isolation between ponds (at least during low tide conditions) and could derive from the existence of local sources of phosphorus. This possibility is sustained by previous reports on P inputs from phosphorite deposits in the area (e.g. P deposits at San Juan de La Costa locality, Hausback, 1984, Álvarez Arellano and Páez Osuna, 1995). In these tidal pools, P inputs likely drove the differences of the nutrient proportions: overall low DIN:P-PO$_4^{-3}$, TN:TP (Table 1) that in general suggested nitrogen limitation, just as the biomass N$_{org}$:P$_{org}$ ratios did. nMDS analyses were useful to distinguish the relevant contributions of temperature and the nutrient environment as the parameters more related to microbiota seasonal dynamics (Fig. 5).

The heterogeneity between ponds of the TN:TP and DIN:P-PO$_4^{-3}$ ratios in the pool-water contrasts with a consistent (and significant between seasons) lower N$_{org}$:P$_{org}$ ratio in algal biomass during summertime, suggesting that nitrogen was more limiting then, compared to the winter sampling.

4.2. Microstructural signals to understand microbial habitats

4.2.1. Biomineralization in the algal holobiont
While Mg-carbonate is the main carbonate reported in rhodophyta structures (e.g., Diaz-Pulido et al., 2014), there is evidence that CA metabolism (e.g., related to reproduction) influences the spatial allocation of carbonates, e.g., aragonite infilling the conceptacle (Krayesky-Self et al., 2016).

Our SR-FTIR spectromicroscopy observations of the fresh surface of summer *N. trichotomum* allowed us to determine that Mg-calcite and aragonite exhibit spatial segregation within the carbonate structure of the algal perithallus (Fig. 3B). Additionally, we detected the localization of sulfated polysaccharides within these hexagonal chambers formed by thin carbonated walls. Previous studies address that this type of polysaccharides might constitute around 70% of the dry matter in red algae (McCandless and Craigie, 1979) and have potential roles in biomineralization (Arias et al., 2004). A spatial map of the relative proportion between polysaccharides and proteins shows a higher content of polysaccharides, particularly in some central areas (red colored) of the algal cell. In the perithallus cell, infrared bands typically related to prokaryotic membranes (~2750 to ~3000 cm^{-1}) had low contribution. This fact illustrates that algal tissue was dominating the cell content.

Morphogenesis of carbonated structures of rhodophyta is complex and diverse (Cabioch, 1988) and includes transitory phases of unknown periodicity, such as sloughing (i.e., periodically shedding a surface layer against marine fouling). Our SR-FTIR analyses of the scraped layer of the epithallus (Fig. 3A) match previous descriptions and potential function of a sloughing layer (Littler and Littler, 1999). This comprised a more complex mineral diversity, represented by carbonates and silica (3-dimensional and layered silicates as described by FTIR analyses). The signals of living biomass are less conspicuous in this layer, compared to epithallus cells (particularly proteins at ~1540 cm^{-1} band, but also

polysaccharides at ~1045 cm^{-1} band), only visible in the thinner area. Sloughing has been described in different species of *Neogoniolithon* as an effective anti-fouling strategy to avoid algal (such as diatoms) and particulate materials deposition (Littler and Littler, 1999; Gomez-Lemos and Diaz-Pulido, 2017). Our results show this shedding-layer comprises a mix of mineral materials including silica, as reported for example in marine calcifying mats, potentially related to microbial activity (Tazaki, 1997). Signals of organic molecules found in the epithallus structure were associated with silicates, as described by Valdespino-Castillo et al. (2018) in diverse calcifying microbial mats (at ~1540 cm^{-1} and ~ 2900 cm^{-1}, described as heterocyclic organic compounds —H and -CH bonded to layer silicates (see Farmer, 1975; Henning, 1975; Kuang et al., 2016).

4.2.2. High magnesium calcites and ankerite characterize the mineral thallus of N. trichotomum

Our findings of a slightly higher content of magnesium in calcites during the summertime (18% vs. 19% mol, Section 3.2.1 XRD + Rietveld) concur with those from Adey et al. (2013) who reported higher Mg in parts of rhodophyta crusts of *Clathromorphum compactum* and *C. nereostratum* that have grown faster during the warmer seasons. More studies are required to clarify the effect of temperature in the Mg-content of Rhodophyta carbonates, particularly after recent studies associate Mg-allocation with morphological changes of rhodophyta thalli and not with temperature (Nash and Adey, 2018).

Recent studies try to address the pCO$_2$ resisting threshold of Mg content in calcite in order to understand coralline algae resistance to ocean acidification. A cross-comparison study conducted by Nash et al. (2013) showed Mg-calcite with higher Mg content (17.27–18 mol% MgCO$_3$) undergo less dissolution than coralline structures with less Mg content. Along with this finding, ankerite is a mineral in the group of dolomites, which are rhombohedral carbonates with higher thermodynamic stability (and less solubility) than Mg-calcite (Nash et al., 2013). The boundary between dolomite and ankerite is arbitrarily set at 20 mol% CaFe(CO$_3$)$_2$ (Krupka et al., 2010). Accordingly, the structural Mg-carbonates described here for *N. trichotomum* (Mg calcite >18 mol%) exhibit potential resistance to dissolution in a higher-pCO$_2$ world. This assumption requires further experimental testing because large uncertainties remain to understand the role of microbes and embedded organic matter in the solubility of magnesian calcite (Morse and Arvidson, 2002).

While structural carbonate formation is related to ontogeny (and probably to metabolic changes), it is likely also related to the presence of a dynamic microbiota, as we explore here. Bacteria changing between summer and winter in *N. trichotomum* included cyanobacterial groups (Fig. 5), which are recognized phototrophs driving redox diel gradients related to calcium carbonate precipitation at microscale (Ries, 2010; Hofmann et al., 2018).

Iron carbonates have been found as components of biomineralizations of different aquatic environments, the recent reports of siderite in low to neutral pH (Sánchez-Román et al., 2014) expanded our knowledge about carbonates precipitation, until recently considered restricted to high pH environments (Stumm and Morgan, 1996; Morse and Arvidson, 2002). The formation of iron carbonates in sediments of the Rio Tinto is related to the microbial reduction of the ferric iron coupled to the oxidation of organic compounds (Sánchez-Román et al., 2014). In our study area, no terrigenous (iron) sources have been recognized or described close to the studied pools, suggesting that *N. trichotomum* (and its microbiota) may play a specific role mediating iron precipitation. Among various microbial families and genera linked to the formation of iron minerals (Luu and Ramsay, 2003), *Ferrimonas* (Alteromonadales), was the detected microbe found in *N. trichotomum* microbiota (0.03–1.54% of relative abundance in algal samples). This gamma proteobacterium has been described to perform iron reduction of Fe (III) with H$_2$ or organic acids serving as the electron donor (Lovley, 2000) and nitrate-reduction and denitrification in marine environments (McMeekin, 2015). *Desulfopila,* also found in the algal microbiota, is capable of taking electrons directly from elemental iron under anoxic conditions (Beese-Vasbender et al., 2015), exhibiting a relative abundance of 0.05–0.25% in algal samples (of summer), this microbe is also potentially involved in iron cycling within the algal thallus. Some members of Desulfobacteraceae and Desulfobulbaceae might also be contributing to iron cycling within *N. trichotomum*, they exhibit low abundance (0.1–0.23% and 0.17–1% of relative abundance in algal samples).

4.2.3. Potassium evaporite minerals suggest the presence of halophilic microhabitats in the algal holobiont

Potassium and magnesium (chloride) minerals found in the algal calcarean bioconstructions (sylvite and bischofite, respectively) are soft and much more soluble than halite (NaCl). Their presence has been related to advanced evaporation stages (e.g. in Álvarez et al., 2016), for example in brine environments where CaCl$_2$ is abundant and MgSO$_4$ is not formed (Davison, 2007) or in evaporite minerals of Mars resulting from basalt weathering (Tosca and McLennan, 2006). These "potash" salts entail a strong indication that microbes might have to cope with halophilic conditions within the algal thallus. Our findings of a collection of previously described halotolerant and halophilic bacteria in the algal microbiome support this suggestion. Actually, the selected bacterial families that explain microbial communities seasonal change comprise known halophilic genera such as *Hahella* (Baik et al., 2005), *Granulosicoccus*, (Lee et al., 2007), or *Ferrimonas* (Katsuta et al., 2005). *Granulosicoccus* has been isolated from algae and sponges and detected as part of the core microbiome of the rhodophyta *Porphyra umbilicalis* (Miranda et al., 2013). Nostocaceae, more abundant in the summer, comprises genera also related to halophilia in calcifying systems: *Calhotrix, Cylindrospermopsis* and *Rivularia*, which have been described in hypersaline lakes (Gómez et al., 2020). Other examples are shown in Supplementary Fig. S3, e.g., *Woeseia* (Zhang et al., 2019), *Alkalispirochaeta* (Sravanthi et al., 2016) and *Salinispira* (Hania et al., 2015). Halophilic and/or halotolerant microorganisms might play important ecological roles in algal adaptation and resilience that should be studied. *Woeseia* (found here in both seasons) has been related to copper resistance in areas with low oxygen availability (Zhang et al., 2019); this microbe participates in hydrocarbon degradation as well (Bacosa et al., 2018). These characteristics are being explored as targets for biotechnology and bioremediation studies. *Granulosicoccus*, and *Maribacter (*Flavobacteriaceae) have been reported to be relevant taxa for oil spills bioremediation (Sun et al., 2020). *Maribacter* has been also reported as halophilic iron oxidizer (Bonis and Gralnick, 2015; Jackson et al., 2015). This microbe has been isolated from marine sponges, reported to perform sulfate reduction, and to exhibit adaptive mechanisms to ultra-oligotrophic environments (Xu et al., 2015; Yoon et al., 2011).

4.3. N. trichotomum hosts seasonally dynamic bacterial communities

N. trichotomum microbiota harbored microbial groups reported before in coralline rhodophyta (Webster et al., 2011; Cavalcanti et al., 2014; Quéré et al., 2019). Some of the main groups reported by Cavalcanti et al. (2014), who studied the Rhodophyta-dominated Abrolhos rhodolith beds, were also found in our results (Alteromonadales, Chromatiales, Oceanospirillales, Myxococcales, Burkholderiales, Rhodo bacterales, Sphingomonadales, Rhodospirillales, and Rhizobiales), but other, such as Caulobacterales, Nitrosomonadales, Methylophiliales, Desulfobacterales, and Enterobacterales were absent. As found in other reports for these rhodoliths (Cavalcanti et al., 2014), *N. trichotomum* microbiota found here was diverse and distinctive from that of its surrounding water. A large part of the algal microbiota comprised low-abundance microbial groups and, although a longer-term survey is necessary to further clarify their dynamics, intra sample-diversity indicates low abundance groups might vary among individual algae of the same species, as stated by (Hester et al., 2016). In their review of the microbiota of macroalgae, Florez et al. (2017) described some microbial phyla found in Rhodophyta

but absent in other macroalgae, which include Aquificae, Chlorobi, Dyctioglomi, Lentisphaerae, and Tenericutes. Among them, only some sequences of Lentisphaerae and Tenericutes were recovered within *N. trichotomum,* but a larger diversity was found in pool water.

Alphaproteobacteria, Gammaproteobacteria and Bacteroidetes are groups whose abundance has been reported to change when different species of *Neogoniolithon* face thermal stress (Webster et al., 2011) or high-temperature related diseases (Meistertzheim et al., 2017; Quéré et al., 2019). Our results showed that Gammaproteobacteria increase from winter to summer in all the algal samples. In contrast, Alphaproteobacteria abundance decreased from winter to summer in all samples, and Bacteroidetes did not show a significant seasonal pattern.

4.4. Bacterial associates may support adaptive responses of the algal holobiont to changes in temperature and nutrient levels

Bacterial genera that better-explain algal microbiota dynamics and environmental thresholds have been previously reported as halotolerant or halophilic microbes (Supplementary Fig. S3). Additionally, some of these bacterial genera have been previously described as oligotrophic phototrophs which tolerate high desiccation, extreme temperatures and radiation (e.g., the Xenococcaceae *Chrococcidiopsis* and some Nostocaceae; Fagliarone et al., 2017, Gómez et al., 2020). Gammaproteobacterial taxa such as *Hahella*, and clade BD1–7 (placed in the warmer, less-silicate region of the MRT model); together with gammaproteobacterial OM60 clade, they have been recognized also as marine oligotrophs (Oh et al., 2010). The genus *Richelia* (Nostocaceae) was also found. *Richelia intracellularis* has been reported as a diazotrophic cyanobacterial symbiont of the diatom *Rhisozolenia* (Villareal, 1990).

Rhodobacteraceae outstands in the region of cooler temperature and low nitrate availability. Multiple reports address the abundance of this bacterial family in oligotrophic environments (Pujalte et al., 2014; Simon et al., 2017) this bacterial family is represented in this part of the model by genera such as *Roseobacter, Lentibacter, Sulfitobacter* and *Loktanella*, which are halophilic and marine species capable of oxidizing sulfite (Pujalte et al., 2014). *Ferrimonas sediminum* as well as Rhodobacteraceae *Loktanella sediminum* and *Tateyamaria omphalii* have been isolated from healthy (Quéré et al., 2019) compared to white band diseased *Neogoniolithon brassica-florida*. *Silicimonas,* also found in *N. trichotomum*, has been isolated from the marine diatom *Thalassiosira delicatula* who has been related to sulfur oxidation and phosphonate utilization (Crenn et al., 2019). *Granulosicoccus*, a known halophilic microbe (Lee et al., 2007), is represented by Thialorhabdaceae in the lower temperature, higher nitrate region. *Chroococcidiopsis* (Xenococcaceae), found in the cooler, lower nutrient region, has also been found inhabiting endolithic and carbonate forming mats (Valdespino-Castillo et al., 2018; Sánchez-Sánchez et al., 2019).

5. Conclusions

High Mg calcites and iron carbonates were found, and spatially described at microscale, in the microbially mediated mineral structure of *N. trichotomum*. The potential resistance of these minerals to dissolution in a higher pCO_2 world pinpoint coralline algae as targets to assess and predict coastal resilience. Concurrently finding potassium evaporite minerals and a marked abundance (and diversity) of halophilic and halotolerant microbes provided an integrated suggestion of the existence of halophilic microhabitats within the algal thallus. Prokaryotic communities' seasonal dynamics was related mainly to temperature and nutrient thresholds; these environmental factors were correlated with specific taxa that might be key factors in the holobiontic thermal and nutrient adaptive responses. Finally, the complex interactions between Rhodophyta and microbes are likely related to the past evolutionary success of Rhodophyta, and potentially involved in the fate of coralline habitats and future coastal morphology.

CRediT authorship contribution statement

Patricia M. Valdespino-Castillo: Conceptualization, Methodology, Data curation, Formal analysis, Writing-Original draft preparation, Funding acquisition. **Andrea Bautista-García**: Conceptualization, Methodology, Data curation, Formal analysis, Writing-Original draft preparation. **Fabio Favoretto:** Conceptualization, Methodology, Data curation, Formal analysis, Writing - review & editing. **Martín Merino-Ibarra:** Resources, Data curation, Formal analysis, Funding acquisition, Writing - review & editing. **Rocío J. Alcántara-Hernández:** Data curation, Formal analysis, Funding acquisition, Writing - review & editing. **Teresa Pi-Puig:** Data curation, Formal analysis, Technical assistance, Writing - review & editing. **F. Sergio Castillo:** Methodology, Technical assistance: Formal analysis, Writing - review & editing. **Silvia Espinosa-Matías:** Methodology, Technical assistance, Microscopy images, Formal analysis, Writing - review & editing. **Hoi-Ying Holman:** Resources, Methodology, Data curation, Formal analysis, Funding acquisition, Writing - review & editing. **Anidia Blanco-Jarvio**: Conceptualization, Methodology, Resources, Formal analysis, Funding acquisition, Writing-Original draft preparation.

Declaration of competing interest

The authors declare that they have no known competing financial interests or personal relationships that could have appeared to influence the work reported in this paper.

Appendix A. Supplementary data

Supplementary data to this article can be found online at https://doi.org/10.1016/j.scitotenv.2020.143877.

References

Adey, W. H., Halfar, J., & Williams, B. (2013). The coralline genus Clathromorphum foslie emend. Adey: biological, physiological, and ecological factors controlling carbonate production in an arctic-subarctic climate archive. Doi:https://doi.org/10.5479/si.1943667X.40.1.

Aguirre, J., Riding, R., Braga, J.C., 2000. Diversity of coralline red algae: origination and extinction patterns from the Early Cretaceous to the Pleistocene. Paleobiology 26, 651–667. https://doi.org/10.1666/0094-8373(2000)026<0651:DOCRAO>2.0.CO;2.

Álvarez Arellano, A., Páez Osuna, F., 1995. Estudio geoquímico de siete muestras de las formaciones fosfáticas del sur de la península de Baja California, México. Geofís. Int. 34, 411–416.

Álvarez, M., Carol, E., & Bouza, P. J. (2016). Precipitation/dissolution of marine evaporites as determinants in groundwater chemistry in a salt marsh (Península Valdés, Argentina). Marine Chemistry, 187, 35-42. doi:10.1016/j.marchem.2016.10.005.

Andersen, F.A., Brecevic, L., 1991. Infrared spectra of amorphous and crystalline calcium carbonate. Acta Chem. Scand 45 (10), 1018–1024.

Arias, J.L., Neira-Carrillo, A., Arias, J.I., Escobar, C., Bodero, M., David, M., Fernández, M.S., 2004. Sulfated polymers in biological mineralization: a plausible source for bio-inspired engineering. J. Mater. Chem. 14 (14), 2154–2160. https://doi.org/10.1039/B401396D.

Bacosa, H.P., Erdner, D.L., Rosenheim, B.E., Shetty, P., Seitz, K.W., Baker, B.J., Liu, Z., 2018. Hydrocarbon degradation and response of seafloor sediment bacterial community in the northern Gulf of Mexico to light Louisiana sweet crude oil. The ISME journal 12 (10), 2532–2543. https://doi.org/10.1038/s41396-018-0190-1.

Baik, K.S., Seong, C.N., Kim, E.M., Yi, H., Bae, K.S., Chun, J., 2005. Hahella ganghwensis sp. nov., isolated from tidal flat sediment. Int. J. Syst. Evol. Microbiol. 55 (2), 681–684. https://doi.org/10.1099/ijs.0.63411-0.

Baquiran, J.I.P., Nada, M.A.L., Posadas, N., Manogan, D.P., Cabaitan, P.C., Conaco, C., 2020. Population structure and microbial community diversity of two common tetillid sponges in a tropical reef lagoon. PeerJ 8, e9017. https://doi.org/10.7717/peerj.9017.

Beese-Vasbender, P.F., Nayak, S., Erbe, A., Stratmann, M., Mayrhofer, K.J., 2015. Electrochemical characterization of direct electron uptake in electrical microbially influenced corrosion of iron by the lithoautotrophic SRB Desulfopila corrodens strain IS4. Electrochim. Acta 167, 321–329. https://doi.org/10.1016/j.electacta.2015.03.184.

Bolyen, E., Rideout, J.R., Dillon, M.R., et al., 2019. Reproducible, interactive, scalable and extensible microbiome data science using QIIME 2. Nat. Biotechnol. 37, 852–857. https://doi.org/10.1038/s41587-019-0209-9.

Bonis, B.M., Gralnick, J.A., 2015. Marinobacter subterrani, a genetically tractable neutrophilic Fe (II)-oxidizing strain isolated from the Soudan Iron Mine. Front. Microbiol. 6, 719. https://doi.org/10.3389/fmicb.2015.00719.

Cabioch, J., 1988. Morphogenesis and generic concepts in coralline algae—a reappraisal. Helgoländer Meeresuntersuchungen 42 (3), 493–509.

Callahan, B.J., McMurdie, P.J., Rosen, M.J., Han, A.W., Johnson, A.J.A., Holmes, S.P., 2016. DADA2: high-resolution sample inference from Illumina amplicon data. Nat. Methods 13 (7), 581. https://doi.org/10.1038/nmeth.3869.

Caporaso, J.G., Kuczynski, J., Stombaugh, J., Bittinger, K., Bushman, F.D., Costello, E.K., et al., 2010. QIIME allows analysis of high-throughput community sequencing data. Nat. Methods 7 (5), 335–336. https://doi.org/10.1038/nmeth.f.303.

Caporaso, J.G., Lauber, C.L., Walters, W., 2012. a, Berg-Lyons D, Huntley J, Fierer N, et al. Ultra-high-throughput microbial community analysis on the Illumina HiSeq and MiSeq platforms. ISME J 6, 1621–1624. https://doi.org/10.1038/ismej.2012.8.

Cavalcanti, G.S., Gregoracci, G.B., Dos Santos, E.O., Silveira, C.B., Meirelles, P.M., Longo, L., Gotoh, K., Nakamura, S., Iida, T., Sawabe, T., Rezende, C.E., Francini-Filho, R.B., Moura, R.L., Amado-Filho, G.M., Rezende, C.E., 2014. Physiologic and metagenomic attributes of the rhodoliths forming the largest CaCO 3 bed in the South Atlantic Ocean. The ISME journal 8 (1), 52. https://doi.org/10.1038/ismej.2013.133.

Cavalcanti, G.S., Shukla, P., Morris, M., Ribeiro, B., Foley, M., Doane, M.P., Edwards, M., Dinsdale, E., Thompson, F.L., 2018. Rhodoliths holobionts in a changing ocean: host-microbes interactions mediate coralline algae resilience under ocean acidification. BMC Genomics 19 (1), 701. https://doi.org/10.1186/s12864-018-5064-4.

Coria-Monter, E., Monreal-Gómez, M.A., de León, D.A.S., Durán-Campos, E., Merino-Ibarra, M., 2017. Wind driven nutrient and subsurface chlorophyll-a enhancement in the Bay of La Paz, Gulf of California. Estuar. Coast. Shelf Sci. 196, 290–300. https://doi.org/10.1016/j.ecss.2017.07.010.

Cornwall, C.E., Diaz-Pulido, G., Comeau, S., 2019. Impacts of ocean warming on coralline algal calcification: meta-analysis, knowledge gaps, and key recommendations for future research. Front. Mar. Sci. 6, 186. https://doi.org/10.3389/fmars.2019.00186.

Crenn, K., Bunk, B., Spröer, C., Overmann, J., Jeanthon, C., 2019. Complete genome sequence of the silicimonas algicola type strain, a representative of the marine Roseobacter group isolated from the cell surface of the marine diatom Thalassiosira delicatula. Microbiology resource announcements 8 (9).

Cruz-Ayala, M.B., Núñez-López, R.A., López, G.E., 2001. Seaweeds in the southern Gulf of California. Bot. Mar. 44 (2), 187–197. https://doi.org/10.1515/BOT.2001.025.

Davison, I., 2007. Geology and tectonics of the South Atlantic Brazilian salt basins. Geol. Soc. Lond., Spec. Publ. 272 (1), 345–359. https://doi.org/10.1144/GSL.SP.2007.272.01.18.

De'Ath, G., 2002. Multivariate regression trees: a new technique for modeling species–environment relationships. Ecology 83 (4), 1105–1117. https://doi.org/10.1890/0012-9658(2002)083[1105:MRTANT]2.0.CO;2.

Diaz-Pulido, G., Nash, M.C., Anthony, K.R., Bender, D., Opdyke, B.N., Reyes-Nivia, C., Troitzsch, U., 2014. Greenhouse conditions induce mineralogical changes and dolomite accumulation in coralline algae on tropical reefs. Nat. Commun. 5, 3310. https://doi.org/10.1038/ncomms4310.

Fagliarone, C., Mosca, C., Ubaldi, I., Verseux, C., Baqué, M., Wilmotte, A., Billi, D., 2017. Avoidance of protein oxidation correlates with the desiccation and radiation

resistance of hot and cold desert strains of the cyanobacterium Chroococcidiopsis. Extremophiles 21 (6), 981–991. https://doi.org/10.1007/s00792-017-0957-8.

Farmer, V. C. (1975). "The layer silicates," in The Infrared Spectra of Minerals, ed V. C. Farmer (London: Mineral Society), 331–363.

Florez, J.Z., Camus, C., Hengst, M.B., Buschmann, A.H., 2017. A functional perspective analysis of macroalgae and epiphytic bacterial community interaction. Front. Microbiol. 8, 2561. https://doi.org/10.3389/fmicb.2017.02561.

Foster, M.S., 2001. Rhodoliths: between rocks and soft places. J. Phycol. 37 (5), 659–667. https://doi.org/10.1046/j.1529-8817.2001.00195.x.

Fredericq, S., Krayesky-Self, S., Sauvage, T., Richards, J., Kittle, R., Arakaki, N., Hickerson, E., Schmidt, W.E., 2019. The critical importance of rhodoliths in the life cycle completion of both macro-and microalgae, and as holobionts for the establishment and maintenance of marine biodiversity. Front. Mar. Sci. 5, 502. https://doi.org/10.3389/fmars.2018.00502.

Gómez, F.J., Boidi, F.J., Mlewski, E.C., Gérard, E., 2020. The Carbonate System in Hypersaline Lakes: The Case of Laguna Negra (in the Puna Region of Catamarca, Argentina). In Microbial Ecosystems in Central Andes Extreme Environments (Pp. 231–242) Springer, Cham https://doi.org/10.1007/978-3-030-36192-1_16.

Gomez-Lemos, L.A., Diaz-Pulido, G., 2017. Crustose coralline algae and associated microbial biofilms deter seaweed settlement on coral reefs. Coral Reefs 36 (2), 453–462. https://doi.org/10.1007/s00338-017-1549-x.

Grasshoff, K., Kremling, K., Ehrhardt, M. (Eds.), 1999. Methods of Seawater Analysis. John Wiley & Sons https://doi.org/10.1002/9783527613984.

Hania, W. B., Joseph, M., Schumann, P., Bunk, B., Fiebig, A., Spröer, C., ... & Spring, S. (2015). Complete genome sequence and description of Salinispira pacifica gen. nov., sp. nov., a novel spirochaete isolated form a hypersaline microbial mat. Standards in genomic sciences, 10(1), 7. doi:https://doi.org/10.1186/1944-3277-10-7.

Hausback, B.P., 1984. Cenozoic Volcanic and Tectonic Evolution of Baja California Sur, Mexico. SEPM, AAPG.

Henning, O. (1975). "Cements; The hydrated silicates and aluminates," in The Infrared Spectra of Minerals, ed V. C. Farmer (London: Mineral Society), 445–464.

Hester, E.R., Barott, K.L., Nulton, J., Vermeij, M.J., Rohwer, F.L., 2016. Stable and sporadic symbiotic communities of coral and algal holobionts. The ISME journal 10 (5), 1157. https://doi.org/10.1038/ismej.2015.190.

Higgins, H.G., Stewart, C.M., Harrington, K.J., 1961. Infrared spectra of cellulose and related polysaccharides. J. Polym. Sci. 51 (155), 59–84. https://doi.org/10.1002/pol.1961.1205115505.

Hinojosa-Arango, G., Riosmena-Rodríguez, R., 2004. Influence of Rhodolith-forming species and growth-form on associated fauna of rhodolith beds in the central-west Gulf of California, México. Mar. Ecol. 25 (2), 109–127. https://doi.org/10.1111/j.1439-0485.2004.00019.x.

Hofmann, L.C., Heiden, J., Bischof, K., Teichberg, M., 2014. Nutrient availability affects the response of the calcifying chlorophyte Halimeda opuntia (L.) JV Lamouroux to low pH. Planta 239 (1), 231–242.

Hofmann, L.C., Schoenrock, K., De Beer, D., 2018. Arctic coralline algae elevate surface pH and carbonate in the dark. Front. Plant Sci. 9, 1416. https://doi.org/10.3389/fpls.2018.01416.

Holman, H.Y.N., Perry, D.L., Martin, M.C., Lamble, G.M., McKinney, W.R., Hunter-Cevera, J.C., 1999. Real-time characterization of biogeochemical reduction of Cr(VI) on basalt surfaces by SR-FTIR imaging. Geomicrobiol J. 16 (4), 307–324. https://doi.org/10.1080/014904599270569.

Jackson, S.A., Kennedy, J., Morrissey, J.P., O'Gara, F., Dobson, A.D., 2015. Maribacter spongiicola sp. nov. and Maribacter vaceletii sp. nov., isolated from marine sponges, and emended description of the genus Maribacter. Int. J. Syst. Evol. Microbiol. 65 (7), 2097–2103. https://doi.org/10.1099/ijs.0.000224.

Kato, A., Baba, M., Suda, S., 2013. Taxonomic circumscription of heterogeneous species N eogoniolithon brassica-Florida (Corallinales, Rhodophyta) in Japan. Phycol. Res. 61 (1), 15–26. https://doi.org/10.1111/j.1440-1835.2012.00665.x.

Katsuta, A., Adachi, K., Matsuda, S., Shizuri, Y., Kasai, H., 2005. Ferrimonas marina sp. nov. Int. J. Syst. Evol. Microbiol. 55 (5), 1851–1855. https://doi.org/10.1099/ijs.0.63689-0.

Kirkwood, D.S., 1994. Sanplus Segmented Flow Analyzer and its Applications. Seawater analysis. Skalar, Amsterdam.

Krayesky-Self, S., Richards, J.L., Rahmatian, M., Fredericq, S., 2016. Aragonite infill in overgrown conceptacles of coralline Lithothamnion spp.(Hapalidiaceae, Hapalidiales, Rhodophyta): new insights in biomineralization and phylomineralogy. J. Phycol. 52 (2), 161–173. https://doi.org/10.1111/jpy.12392.

Krupka, K. M., Cantrell, K. J., & McGrail, B. P. (2010). Thermodynamic data for geochemical modeling of carbonate reactions associated with CO2 sequestration–Literature review (No. PNNL-19766). Pacific Northwest National Lab.(PNNL), Richland, WA (United States).doi: https://doi.org/10.2172/992369.

Kuang, X., Shao, J., Chen, A., Luo, S., Peng, L., Wu, G., et al., 2016. Effects of bloom-forming cyanobacterial extracellular polymeric substances on the adsorption of cadmium onto kaolinite: behaviors and possible mechanisms. SpringerPlus 5, 542. https://doi.org/10.1186/s40064-016-2191-8.

Lee, K., Lee, H. K., Choi, T., Kim, K., & Cho, J. (2007). Granulosicoccaceae fam. nov., to include Granulosicoccus antarcticus gen. nov., sp. nov., a non-phototrophic, obligately aerobic chemoheterotroph inspaña. 1136p.

Littler, M.M., Littler, D.S., 1999. Epithallus sloughing: a self-cleaning mechanism for coralline algae. Coral Reefs 18, 204. https://doi.org/10.1007/s003380050182.

Lovley, D., 2000. Fe(III) and Mn(IV) reduction. In: Lovley, D. (Ed.), Environmental Microbe-Metal Interactions. ASM Press, Washington, DC, pp. 3–30 https://doi.org/10.1128/9781555818098.ch1.

Luu, Y.S., Ramsay, J.A., 2003. Microbial mechanisms of accessing insoluble Fe (III) as an energy source. World J. Microbiol. Biotechnol. 19 (2), 215–225. https://doi.org/10.1023/A:1023225521311.

McCandless, E.L., Craigie, J.S., 1979. Sulfated polysaccharides in red and brown algae. Annu. Rev. Plant Physiol. 30 (1), 41–53. https://doi.org/10.1146/annurev.pp.30.060179.000353.

McCoy, S.J., Kamenos, N.A., 2015. Coralline algae (Rhodophyta) in a changing world: integrating ecological, physiological, and geochemical responses to global change. J. Phycol. 51 (1), 6–24. https://doi.org/10.1111/jpy.12262.

McMeekin 2015. Alteromonadaceae In *Bergey's Manual of Systematics of Archaea and Bacteria.* Bowman, J. P., & McMeekin, T. A. (2015)., 1–2.

Meistertzheim, A.L., Nugues, M.M., Quéré, G., Galand, P.E., 2017. Pathobiomes differ between two diseases affecting reef building coralline algae. Front. Microbiol. 8, 1686. https://doi.org/10.3389/fmicb.2017.01686.

Merino, M., 1987. The coastal zone of Mexico. Coast. Manag. 15 (1), 27–42. https://doi.org/10.1080/08920758709362014.

Miranda, L.N., Hutchison, K., Grossman, A.R., Brawley, S.H., 2013. Diversity and abundance of the bacterial community of the red macroalga Porphyra umbilicalis: did bacterial farmers produce macroalgae? PLoS One 8 (3), e58269. https://doi.org/10.1371/journal.pone.0058269.

Morse, J.W., Arvidson, R.S., 2002. The dissolution kinetics of major sedimentary carbonate minerals. Earth Sci. Rev. 58 (1–2), 51–84. https://doi.org/10.1016/S0012-8252(01)00083-6.

Nash, M.C., Adey, W., 2018. Anatomical structure overrides temperature controls on magnesium uptake–calcification in the Arctic/subarctic coralline algae Leptophytum laeve and Kvaleya epilaeve (Rhodophyta; Corallinales). Biogeosciences 15 (3), 781. https://doi.org/10.5194/bg-15-781-2018.

Nash, M.C., Opdyke, B.N., Troitzsch, U., Russell, B.D., Adey, W.H., Kato, A., ... Kline, D.I., 2013. Dolomite-rich coralline algae in reefs resist dissolution in acidified conditions. Nature climate change 3 (3), 268–272. https://doi.org/10.1038/nclimate1760.

Nash, M.C., Diaz-Pulido, G., Harvey, A.S., Adey, W., 2019. Coralline algal calcification: a morphological and process-based understanding. PLoS One 14 (9). https://doi.org/10.1371/journal.pone.0221396.

Nelson, W.A., 2009. Calcified macroalgae - critical to coastal ecosystems and vulnerable to change: a review. Mar. Freshw. Res. 60, 787–801. https://doi.org/10.1071/MF08335.

Oh, H.M., Kim, H., Kim, K.M., Min, G.S., Cho, J.C., 2010. Porticoccus litoralis gen. nov., sp. nov., a gammaproteobacterium isolated from the Yellow Sea. Int. J. Syst. Evol. Microbiol. 60 (4), 727–732. https://doi.org/10.1099/ijs.0.013938-0.

Oksanen, J., Blanchet, F. G., Friendly, M., Kindt, R., Legendre, P., McGlinn, D., ... & Solymos, P. (2019). vegan: Community Ecology Package. R package version 2.5–6. 2019. https://CRAN.R-project.org/package=vegan.

Perkins, R.G., Williamson, C.J., Brodie, J., Barillé, L., Launeau, P., Lavaud, J., Yallop, M., Jesus, B., 2016. Microspatial variability in community structure and photophysiology of calcified macroalgal microbiomes revealed by coupling of hyperspectral and high-resolution fluorescence imaging. Sci. Rep. 6, 22343. https://doi.org/10.1038/srep22343.

Planas, D., Agustí, S., Duarte, C.M., Granata, T.C., Merino, M., 1999. Nitrate uptake and diffusive nitrate supply in the Central Atlantic. Limnol. Oceanogr. 44 (1), 116–126. https://doi.org/10.4319/lo.1999.44.1.0116.

Porzio, L., Buia, M.C., Ferretti, V., Lorenti, M., Rossi, M., Trifuoggi, M., ... Arena, C., 2018. Photosynthesis and mineralogy of Jania rubens at low pH/high pCO2: A future perspective. Science of The Total Environment 628, 375–383. https://doi.org/10.1016/j.scitotenv.2018.02.065.

Probst, A.J., Holman, H.Y.N., DeSantis, T.Z., Andersen, G.L., Birarda, G., Bechtel, H.A., ... Moissl-Eichinger, C., 2013. Tackling the minority: sulfate-reducing bacteria in an archaea-dominated subsurface biofilm. The ISME journal 7 (3), 635–651. https://doi.org/10.1038/ismej.2012.133.

Pujalte, M.J., Lucena, T., Ruvira, M.A., Arahal, D.R., Macián, M.C., 2014. The family *Rhodobacteraceae*. In: Rosenberg, E., DeLong, E.F., Lory, S., Stackebrandt, E., Thompson, F. (Eds.), The Prokaryotes. Springer, Berlin, Heidelberg https://doi.org/10.1007/978-3-642-30197-1_377.

Quéré, G., Intertaglia, L., PAYRI, C.E., Galand, P.E., 2019. Disease specific bacterial communities in a coralline algae of the northwestern Mediterranean Sea: a combined culture dependent and-independent approach. Front. Microbiol. 10, 1850. https://doi.org/10.3389/fmicb.2019.01850.

R Core Team, 2019. R: A language and environment for statistical computing. R Foundation for Statistical Computing. Austria. URL, Vienna https://www.R-project.org/.

R Studio Team, 2019. RStudio: Integrated Development for R. RStudio, Inc., Boston, MA URL http://www.rstudio.com/.

Reyes-Nivia, C., Diaz-Pulido, G., Dove, S., 2014. Relative roles of endolithic algae and carbonate chemistry variability in the skeletal dissolution of crustose coralline algae. Biogeosciences 11 (17), 4615–4626. https://doi.org/10.5194/bg-11-4615-2014.

Ries, J.B., 2010. Geological and experimental evidence for secular variation in seawater Mg/Ca (calcite-aragonite seas) and its effects on marine biological calcification. Biogeosciences 7 (9), 2795. https://doi.org/10.5194/bg-7-2795-2010.

Rietveld, H. (1969). A profile refinement method for nuclear and magnetic structures. J. appl. Crystallogr. 2 (82), 65-71. doi:https://doi.org/10.1107/s0021889869006558.

Riosmena-Rodríguez, R., López-Calderón, J.M., Mariano-Meléndez, E., Sánchez-Rodríguez, A., Fernández-Garcia, C., 2012. Size and distribution of rhodolith beds in the Loreto Marine Park: their role in coastal processes. J. Coast. Res. 28 (1), 255–260.

Salinas-González, F., Zaytsev, O., Makarov, V., 2003. Formation of thermohaline structure of water in the Bahía de La Paz from summer to autumn. Ciencias Marinas. 29 (1), 51–69.

Sánchez-Román, M., Fernández-Remolar, D., Amils, R., Sánchez-Navas, A., Schmid, T., San Martin-Uriz, P., ... Vasconcelos, C., 2014. Microbial mediated formation of Fe-carbonate minerals under extreme acidic conditions. Scientific Reports 4, 4767. https://doi.org/10.1038/srep04767.

Sánchez-Sánchez, J., Cerca, M., Alcántara-Hernández, R. J., Lozano-Flores, C., Carreón-Freyre, D., Levresse, G., ... & Aranda-Gómez, J. J. (2019). Extant microbial communities in the partially desiccated Rincon de Parangueo maar crater lake in Mexico. FEMS microbiology ecology, 95(5), fiz051.doi:https://doi.org/10.1093/femsec/fiz051.

Simon, M., Scheuner, C., Meier-Kolthoff, J.P., Brinkhoff, T., Wagner-Döbler, I, Ulbrich, M., ... Göker, M., 2017. Phylogenomics of Rhodobacteraceae reveals evolutionary adaptation to marine and non-marine habitats. The ISME journal 11 (6), 1483–1499. https://doi.org/10.1038/ismej.2016.198.

Sravanthi, T., Tushar, L, Sasikala, C., Ramana, C.V., 2016. Alkalispirochaeta cellulosivorans gen. nov., sp. nov., a cellulose-hydrolysing, alkaliphilic, halotolerant bacterium isolated from the gut of a wood-eating cockroach (Cryptocercus punctulatus), and re-classification of four species of Spirochaeta as new combinations within Alkalispirochaeta gen. Nov. Int. J. Syst. Evol. Microbiol. 66 (4), 1612–1619. https://doi.org/10.1099/ijsem.0.000865.

Stanienda-Pilecki, K.J., 2019. The importance of Fourier transform infrared spectroscopy in the identification of carbonate phases differentiated in magnesium content. Spectroscopy 34 (6), 32–42.

Stumm, W., Morgan, J.J., 1996. Aquatic Chemistry, Chemical Equilibria and Rates in Natural Waters. 3rd edition. John Wiley & Sons, Inc., New York.

Sun, Q.L., Sun, Y.L., Sun, Y.Y., Luan, Z.D., Lian, C., 2020. Marinobacter fonticola sp. nov., isolated from deep sea cold seep sediment. Int. J. Syst. Evol. Microbiol. 70 (2), 1172–1177. https://doi.org/10.1099/ijsem.0.003895.

Tazaki, K., 1997. Biomineralization of layer silicates and hydrated Fe/Mn oxides in microbial mats: an electron microscopical study. Clay Clay Miner. 45, 203–212. https://doi.org/10.1346/CCMN.1997.0450208.

Therneau T.M., Atkinson B., (2014) R mvpart: multivariate partitioning. R package version 1.6-2. https://CRAN.R-project.org/package=mvpart.

Tipson, R.S., Cohen, A., 1968. Reaction of some sulfonic esters of D-mannitol with methoxide; synthesis of 2, 3: 4, 5-dianhydro-D-iditol. Carbohydr. Res. 7 (3), 232–243. https://doi.org/10.1016/S0008-6215(00)81197-0.

Titschack, J., Goetz-Neunhoeffer, F., Neubauer, J. (2011). Magnesium quantification in calcite [(Ca,Mg)CO3]by Rietveld-based XRD analysis: revisiting a well-established method. Am. Mineral. 96(7), 1028–1038. doi:https://doi.org/10.2138/am.2011.3665.

Tosca, N.J., McLennan, S.M., 2006. Chemical divides and evaporite assemblages on Mars. Earth Planet. Sci. Lett. 241 (1–2), 21–31. https://doi.org/10.1016/j.epsl.2005.10.021.

Valderrama, J.C., 1981. The simultaneous analysis of total nitrogen and total phosphorus in natural waters. Mar. Chem. 10, 109–122. https://doi.org/10.1016/0304-4203(81)90027-X.

Valdespino-Castillo, P.M., Hu, P., Merino-Ibarra, M., López-Gómez, L.M., Cerqueda-García, D., Zayas, G.D., Pi-Pug, T., Lestayo, J., Holman, H.Y., Falcón, L., 2018. Exploring biogeochemistry and microbial diversity of extant microbialites in Mexico and Cuba. Front. Microbiol. 9, 510. https://doi.org/10.3389/fmicb.2018.00510.

Villareal, T.A., 1990. Laboratory culture and preliminary characterization of the nitrogen-fixing Rhizosolenia-Richelia symbiosis. Mar. Ecol. 11 (2), 117–132. https://doi.org/10.1111/j.1439-0485.1990.tb00233.x.

Webster, N.S., Soo, R., Cobb, R., Negri, A.P., 2011. Elevated seawater temperature causes a microbial shift on crustose coralline algae with implications for the recruitment of coral larvae. The ISME journal 5 (4), 759. https://doi.org/10.1038/ismej.2010.152.

Xu T, Yu M, Lin H, Zhang Z, Liu J, Zhang XH. Genomic insight into Aquimarina longa SW024 T: its ultra-oligotrophic adapting mechanisms and biogeochemical functions. BMC Genomics. 2015;16:772. Published 2015 Oct 12. doi:https://doi.org/10.1186/s12864-015-2005-3.

Yoon, B.J., You, H.S., Lee, D.H., Oh, D.C., 2011. Aquimarina spongiae sp. nov., isolated from marine sponge Halichondria oshoro. Int. J. Syst. Evol. Microbiol. 61 (2), 417–421. https://doi.org/10.1099/ijs.0.022046-0.

Zhang, Y., Ma, Y., Zhang, R., Zhang, B., Zhai, X., Li, W., ... Hou, B., 2019. Metagenomic resolution of functional diversity in copper surface-associated marine biofilms. Frontiers in microbiology 10, 2863. https://doi.org/10.3389/fmicb.2019.02863.